Respiratory Syncytial Virus Infects Regulatory B Cells in Human Neonates via Chemokine Receptor CX3CR1 and Promotes Lung Disease Severity

Dania Zhivaki, Sébastien Lemoine, Annick Lim, Ahsen Morva, Pierre-Olivier Vidalain, Liliane Schandene, Nicoletta Casartelli, Marie-Anne Rameix-Welti, Pierre-Louis Hervé, Edith Dériaud, et al.

Title

Respiratory syncytial virus infects regulatory B cells in human neonates via chemokine receptor CX3CR1 and promotes lung disease severity

Dania Zhivaki[1,2], Sébastien Lemoine[3,4], Annick Lim[5], Ahsen Morva[1], Pierre-Olivier Vidalain[6], Liliane Schandene[7], Nicoletta Casartelli[8,9], Marie-Anne Rameix-Welti[10,11], Pierre-Louis Hervé[12], Edith Dériaud[3,4], Benoit Beitz[13], Maryline Ripaux-Lefevre[13], Jordi Miatello[14,15,16], Brigitte Lemercier[5], Valerie Lorin[17,18], Delphyne Descamps[12], Jenna Fix[12], Jean-François Eléouët[12], Sabine Riffault[12], Olivier Schwartz[8,9], Fabrice Porcheray[13], Françoise Mascart[7,19], Hugo Mouquet[17,18], Xiaoming Zhang[20,21], Pierre Tissières[14,15,16,21] and Richard Lo-Man[1, 21,22]

Affiliations

[1]Neonatal Immunity group, Human histopathology and animal models, Institut Pasteur, Paris, France

[2]Paris 7 Diderot University, Paris, France

[3]Régulation Immunitaire et Vaccinologie, Institut Pasteur, Paris, France

[4]INSERM U1041, France

[5]Departement d'Immunologie, Institut Pasteur, Paris, France

[6]Unité de Génomique virale et vaccination, Institut Pasteur, France

[7]Immunobiology Clinic, Hopital Erasme, Brussels, Belgium

[8]Virus et Immunité, Institut Pasteur, Paris, France

[9]UMR CNRS 3568, France

[10]INSERM U1173, Versailles-Saint-Quentin University, Saint-Quentin en Yvelines, France ;

[11]AP-HP, Laboratoire de Microbiologie, Hôpital Ambroise Paré, Boulogne-Billancourt, France

[12]Unité de Virologie et Immunologie Moléculaires, INRA, Université Paris-Saclay, Jouy-en-Josas, France

[13]Bioaster Microbiology Technology Institute, Paris, France

[14]APHP, Pediatric ICU and Neonatal Medicine, Paris South University Hospitals, Le Kremlin-Bicetre, France

[15]School of Medicine, Paris South University, Le Kremlin-Bicêtre, France

[16]Institute of Integrative Biology of the Cell - UMR 9196, Paris Saclay University, Gif-sur-Yvette, France

[17]Laboratory of Humoral Response to Pathogens, Department of Immunology, Institut Pasteur, Paris, France

[18]INSERM U1222, Paris, France.

[19]Laboratory of Vaccinology and Mucosal Immunity, Université Libre de Bruxelles, Brussels, Belgium

[20]Unit of Innate Defense and Immune Modulation, Key Laboratory of Molecular Virology and Immunology, Institut Pasteur of Shanghai, Chinese Academy of Sciences, Shanghai, China

[21]Co-senior authors

[22]Corresponding author

Contact- Corresponding author

Richard Lo-Man
Neonatal Immunity group
Human histopathology and animal models
28 rue du Docteur Roux
Institut Pasteur, Paris, France
Tel: 33 1 45 68 83 52
Fax: 33 1 45 68 85 40
Email: richard.lo-man@pasteur.fr

Text count: 60, 062 characters

Summary

Respiratory syncytial virus (RSV) is the major cause of lower respiratory tract infections in infants and is characterized by pulmonary infiltration of B cells in fatal cases. We analyzed the B cell compartment in human newborns and identified a population of neonatal regulatory B lymphocytes (nBregs) that produced interleukin 10 (IL-10) in response to RSV infection. The polyreactive B cell receptor of nBregs interacted with RSV protein F and induced upregulation of chemokine receptor CX3CR1. CX3CR1 interacted with RSV glycoprotein G, leading to nBreg infection and IL-10 production that dampened T helper 1 (Th1) cytokine production. In the respiratory tract of neonates with severe RSV-induced acute bronchiolitis, RSV-infected nBreg frequencies correlated with increased viral load and decreased blood memory Th1 cell frequencies. Thus, the frequency of nBregs is predictive of the severity of acute bronchiolitis disease and nBreg activity may constitute an early-life host response that favors microbial pathogenesis.

Introduction

Human respiratory syncytial virus (RSV) is the major cause of lower respiratory tract infections in young infants leading to hospitalization and an increased risk factor for asthma development (Smyth and Openshaw, 2006). The immune system plays a critical role in the pathogenesis of RSV disease, and RSV is associated with the exacerbation of airway inflammation (Castro et al., 2008). In infants, fatal outcomes of primary RSV infection are associated with the pulmonary infiltration of B cells (Reed et al., 2009; Welliver et al., 2007), yet the role of these cells remains to be assessed.

Early-life susceptibility to infection contributes to high mortality rates in children under 5 years of age (Prabhudas et al., 2011) who display biased T helper 2 (Th2) responses (Siegrist, 2001). We previously showed that B cells with regulatory properties (Bregs) in murine neonates dampen innate inflammation and the functions of the dendritic cells (DCs) in a TLR-dependent manner, thereby inhibiting the Th1 responses (Sun et al., 2005; Zhang et al., 2007). Over the past decade, Bregs, which act through IL-10 secretion, have attracted attention in the fields of autoimmunity, transplantation and cancer (Mauri and Bosma, 2012). B cell-derived IL-10 can be induced through activation by CD40 (Mauri et al., 2003), the B cell receptor (BCR) (Fillatreau et al., 2002) or several Toll-like receptors (TLRs) (O'Garra et al., 1992; Zhang et al., 2007). The regulatory activity of IL-10-producing Bregs is essential in the control of DCs (Sun et al., 2005) and inflammatory T cells (Matsushita et al., 2008), and in the induction of T regulatory (Treg) cells (Lemoine et al., 2011). Breg activity is not associated with a single B cell subset but rather develops under various conditions. In mice, regulatory activity has been extended to IL-35-producing B cells

and to plasma cells in the context of inflammatory and bacterial diseases (Shen et al., 2014).

Here, we analyzed the B-cell compartment in human newborns using high-content mass cytometry, transcriptomics and functional studies. We identified a population of neonatal B lymphocytes with immunosuppressive activity (nBregs) through the production of IL-10. We showed that nBregs, which are a target for RSV, are highly permissive to infection because of BCR recognition of RSV F that drove nBreg activation and expression of the chemokine receptor CX3CR1. CX3CR1 interacted with RSV G glycoprotein promoted infection of nBregs to induce IL-10 production. Analysis of clinical samples indicated that nBregs were associated with poor control of RSV infection in neonates. We propose the use of the frequency of nBregs as a prognostic tool to determine bronchiolitis severity and the use of both RSV F and G glycoprotein as targets for the development of interventions in the context of acute infection.

Results

RSV infection activates neonatal Bregs resulting in IL-10 production

To analyze the activity of putative Breg cell activity in healthy human newborns, we first examined neonatal B cells within the cord blood mononuclear cell (CBMC) population using a 35-parameter mass cytometric approach (CyTOF). Within the B cell population, unsupervised analysis using the viSNE algorythm that allows dimensionality reduction (Amir el et al., 2013), we revealed different B subsets with different phenotypes that clustered according to their high expression of CD5 or CD10 and that were associated with distinct sets of B cell markers (Fig. 1A-B and Fig. S1). Mature naive (MN) $CD19^{+}$ B cells were phenotypically defined as being

$CD5^{-}CD10^{-}CD1c^{hi}CD21^{hi}CD45RA^{hi}CD23^{lo}CD24^{int}CD38^{int}IgD^{hi}IgM^{lo/hi}$, although there was some heterogeneity for some markers. Immature transitional B cells (IMT, N°2), basically corresponding to $CD24^{hi}CD38^{hi}$ B cells, were phenotypically defined as being $CD5^{lo}CD10^{+}CD1c^{-}CD21^{-}CD45RA^{int}CD23^{-}CD24^{hi}CD38^{hi}IgD^{int}IgM^{hi}$. We also found an additional, previously undescribed population of $CD5^{hi}$ B cells, phenotypically defined as being $CD5^{hi}CD10^{-}CD1c^{lo}CD21^{int}$ $CD45RA^{int}$ $CD23^{hi}CD24^{lo}$ $CD38^{lo}IgD^{lo}IgM^{lo}$ (N°3) (Fig. 1A). We compared the cytometry profiles for additional CD markers of MN B cells, IMT B cells, and the newly defined $CD5^{hi}$ population to bulk $CD19^{+}CD20^{+}$ B cells and further defined the $CD5^{hi}$ B cell phenotype as $CD43^{+}CD9^{-}CD62L^{-}CD40^{int}DR^{int}CD25^{+/-}CD27^{+/-}CD70^{-}$ (Fig. 1B). Adult blood IMT $CD24^{hi}CD38^{hi}$ B cells have been shown to produce IL-10 in response to CD40 (Blair et al., 2010) or CpG and/or TLR9 activation (Menon et al., 2016). Therefore the abundance of IMT B cells in cord blood suggested that these cells could be a major source of IL-10 in newborns. IMT B cells could be distinguished by CD10 expression with an intermediate cell surface expression of CD5 (Fig. S1A), which accurately matched the high expression of CD24 and CD38 (Fig. 1B). To analyze the functions of newborns B cells, the three cord blood B cell populations were sorted by fluorescence activated cell sorting (FACS) based on cell surface CD5 and CD10 expression (Fig. S1B). Among these cord blood-derived cells, $CD5^{hi}$B cells, but not IMT and MN B cells, produced IL-10 upon 48 h of stimulation with A strain of human RSV (HRSV-A)(MOI=2.5) (Fig. 1C). Based on their IL-10 production, we thus named $CD5^{hi}$B cells neonatal Bregs (nBreg). nBregs were abundant in neonatal blood from preterm and full-term babies and their frequency among total B cells quickly waned with age (Fig. 1D). To determine whether these cells originated from the mothers of the babies or the babies themselves, we performed Fluorescence In Situ

Hybridization (FISH) on nBregs from male babies. FISH detected X and Y chromosomes in all of the nBregs isolated from the cord blood of male babies, indicating that the nBregs were derived from the babies rather than the mothers (Fig. 1E). We then sought to determine the stimuli that can lead to IL-10 production from nBregs. While nBregs made IL-10 in response to HRSV (Figure 1C), the nBregs failed to produce IL-10 following infection with a large panel of RNA or DNA viruses, including influenza A virus (IAV), coronavirus 229E, HIV, HSV-1, HTLV and MV (Fig. S1C). To determine whether the induction of the IL-10 response by HRSV was specific to neonatal B cells, we tested the various adult blood B cell subsets and tested their responsiveness to HRSV. We first peformed CyTOF on adult IMT B cells, memory B cells, marginal zone B (MZB) cells, and naïve B cells. Adult IMT cells displayed a phenotype similar to newborn IMT cells, whereas MZBs cells and memory B cells were phenotypically distinct from nBregs (Fig. S2A). FACS sorted adult memory B cells, MZB cells and IMT cells produced IL-10 in response to R848, a TLR7 agonist, but not in response to HRSV (MOI=2.5) (Fig. S2B). These data indicate that HRSV-activated nBregs may possess unique anti-inflammatory properties. The Th1-Th2 balance is critical at the time of the primary RSV infection, as impaired Th1 priming or a Th2 immunopathology have been shown to determine the outcome of secondary infection (Culley et al., 2002). We thus performed an inflammatory T cell suppression assay, which remains the gold standard for assessing Breg activity. Coculture of RSV-activated nBregs with activated $CD4^+$ Th1 cells inhibited IFN-γ and IL-22, but not TNF-α, cytokine production from the $CD4^+$ T cells (Fig. 2A-C). Using IAV-activated neonatal plasmacytoid DCs (pDCs), we recently showed that type I IFN dependent neonatal Th1 differentiation is induced by the allogeneic immune response (Zhang et al., 2014a). Similarly, RSV-activated

neonatal pDCs induced a predominantly IFN-γ Th1 response that was associated with a mild IL-4 Th2 responses (Fig. 2D-F). To investigate whether nBregs could regulate Th1 response indirectly via pDCs, pDC were cultured alone or with RSV-activated nBregs for 2 days, then these cells were co-culture with naïve T cells for six days post. We observed few pDCs infected by RSV when cultured alone or after coculture with nBregs (Fig. S3A). RSV-activated nBregs were able to inhibit the ability of pDCs to prime a IFN-γ T-cell response in an IL-10-dependent manner (Fig. 2D-F). This was associated with decreased the APC functions of pDCs (HLA-DR and CD80), but not the IFN-α response (Fig. S3B). Altogether, these data demonstrate that the nBregs can be specifically activated by RSV and may control the Th1 responses in an IL-10 dependent manner.

Neonatal Bregs are highly permissive to RSV infection

We further investigated the capacity of RSV to directly activate the immunosuppressive properties of nBregs. RSV induced IL-10 transcription in sorted cord blood nBregs as soon as 6 h after exposure (Fig. 3A). We used a rHRSV-expressing mCherry (rHRSV-Ch) construct (Rameix-Welti et al., 2014), to visualize the virus replication in cells by quantifying the red emitted fluorescence. We found that nBregs were preferentially infected by the virus (Fig. 3B) compared to MN or IMT B cells isolated from cord blood. RSV infection did not affect the viability of nBregs (Fig. S4A). Among adult B-cell subsets, only memory B cells were able to be infected with RSV, but they showed much lower viral replication compared with nBregs. (Fig. S4B). nBregs harboring RSV produced more IL-10 compared to their RSV-negative counterparts (Fig. 3C and D) and only live but not UV-treated RSV induced IL-10 production (Fig. 3E), indicative of a role for viral infection in nBreg activation.

Epithelial cells of the respiratory tract are the major targets of HRSV replication in vivo. We found that nBregs, but not MN and IMT B cells, produced IL-10 and were preferentially infected when cocultured with a RSV-infected human epithelial HEp-2 cell line (Fig. 3F and G). Altogether, these data show that nBregs are specifically permissive to RSV infection and that IL-10 production by nBregs requires their viral infection.

RSV is recognized by IgM and can engage the BCR pathway in nBregs

During steady state or upon RSV-mediated activation, nBregs expressed immunoglobulin M (IgM) and IgD, but not IgA or IgG (Fig. S1B and D). In addition, RSV–nBreg cell specific interactions led to IgM secretion by the majority of IL-10-producing cells (Fig. 3H), suggesting a role for the BCR. To investigate this hypothesis, we used a transcriptomic approach to compare nBregs following TLR (R848), BCR (anti-IgM) or viral (RSV or IAV) activation. Principal component analysis (PCA) and hierarchical clustering showed the similarities and distinctness of the Breg response to different activators (Fig. 4A and B). The transcriptional profiles of nBregs stimulated with anti-IgM (BCR) and RSV were closer than with TLR agonist closely related, indicating that BCR activation could be involved in RSV infection. TLR7 or 8 activation by the R848 agonist did not recapitulate the transcriptional pattern of viral activation. Therefore, RSV RNA sensing by TLR7 or 8 may not be essential for the activation of nBregs and may explain why other RNA viruses did not induced IL-10. In addition, pathway analysis showed that RSV activated nBregs significantly upregulated BCR-related pathways but not TLR-, RIG-I- or CD40-related pathways (Fig. 4C). RSV and BCR activation induced expression of common 534 genes in nBregs, as shown on the Venn diagram in Fig. S5A. Gene set enrichment analysis

(GSEA) analysis of the transcriptome also indicated that BCR pathways were induced in nBregs by RSV compared whereas IAV infection did not specifically induce BCR pathways (Fig. S5C). To confirm that RSV-infected nBregs were triggered through their BCRs, we performed an Igα (CD79a) phospho flow assay. Igα phosphorylation was detected in nBregs 30 min. following treatment with anti-IgM or RSV, but not with R848 or IAV treatment (Fig. 4D and E). All the stimuli activated nBregs, as shown by Erk phosphorylation (Fig. S5D). In conclusion, the above experiments strongly indicate that RSV activation of nBregs is mediated in part by Ig recognition.

To further address the role of the BCR at the level of Ig recognition, we analyzed the IgM secreted by nBreg. nBregs produced 5-fold higher concentrations of IgM than MN cells, and 50-fold higher concentrations than IMT cells (Fig. S6A). This finding was confirmed using ELISPOT in which over 80% were secreting IgM nBregs as compared to 10-15% of MN B cells as assessed (Fig. S6A). IgM produced by nBregs, but not MN or IMT B cells, showed specific binding to RSV particles (Fig. 5A and S6B). The mature HRSV envelope consists of glycoprotein (G), fusion (F) protein and small hydrophobic (SH) protein. We found by ELISA that IgM from nBregs recognized the F fusion protein of HRSV but barely recognized the HIV-1 envelope glycoprotein gp140 (Fig. 5A). These IgM still bound the rHRSV-ΔSH and the rHRSV-ΔG mutants showing that F, but not G or SH, were recognized by the Ig (Fig. S6B). Palivizumab, which is an IgG1 humanized monoclonal antibody that binds to F protein outcompeted the binding of nBreg-derived IgM to RSV in a dose-dependent manner (Fig. 5B). In addition, IgM produced by nBregs, but not by MN or IMT B cells, competitively inhibited RSV infection of nBregs (Fig. 5C). We concluded that the F fusion protein, but not SH and G proteins on the virion contributes to IgM-mediated

recognition of RSV by nBregs. This further reinforced the results from transcriptomics and signaling analyses that indicated the engagement of the BCR in nBregs infection by RSV.

Our results indicated that nBreg Ig recognized RSV in the absence of any previous exposure to the virus. One possible explanation of such a property may rely on polyreactivity of the nBreg-IgM that may have developed *in utero* upon exposure to self-antigens. Compared to neonatal MN-IgM, nBreg-IgM displayed canonical features of polyreactive B cells, including self-antigen recognition (Fig. S6A). To explore the molecular basis of this phenomenon, we compared the different neonatal B cell subsets at the level of their Ig repertoire. There was no bias in the usage of specific Ig heavy chain V genes (IGHV) in the IgM derived from nBregs. However, nBreg IgM exhibited a shorter complementarity determining region 3 (CDR3) for most of the IGHV genes, representing more than 90% of the BCR repertoire (Fig. 5D and Fig. S6C and D). A short CDR3 has been reported for MZB cells (Weller et al., 2008) that do not express CD23 and CD5 (Weill et al., 2009). $CD27^+$ "B1-like cells" were described to have a 14 bp CDR3 (Griffin et al., 2011), whereas the CDR3 of nBregs was a 12.9 bp+/-0.2 in length (Fig. 5D). We identified preferential usage of the IGHJ4 segment associated with IGHD6 in nBregs by analyzing the IGHV3 gene PCR products (Fig. 5E-F and Fig. S6E). Both $CD27^+$ and $CD27^-$nBregs showed similar repertoire characteristics and functional properties, such as eqivelent susceptibility to RSV infection and similar concentrations of IL10 production upon stimulation with RSV (Fig. S6F-G). Therefore, the Ig repertoire analysis of nBregs showed that this population constituted a B cell subset with unique characteristics, presumably resulting from specific selection and/or maintenance processes. In summary, the

repertoire traits, together with the viral particle recognition by nBreg IgM, provide the molecular basis for the activation of the BCR pathway following exposure to RSV.

The RSV G glycoprotein interaction with CX3CR1 is critical to infect nBregs

Because ultraviolet (UV) inactivation of RSV impaired IL-10 production, the polyreactive nature of nBreg-IgM was not sufficient to explain the triggering of nBreg activity by RSV. The G glycoprotein harbors a CX3C chemokine motif capable of chemokine mimicry when interacting with chemokine receptor CX3CR1 (Tripp et al., 2001). This interaction is reported as an important mechanism for RSV binding and infection in human lung epithelial cells (Jeong et al. 2015; Chirkova et al. 2015). Because nBreg exposure to RSV activated chemokine receptor pathways (Fig. 4C), we analyzed CX3CR1 expression on cord blood B cells. CX3CR1 was expressed by monocytes, but not by B cells, including nBregs (Fig. 6A). However, after 48 h of RSV exposure, CX3CR1 was induced on nBregs (Fig. 6B), an effect that was mimicked by BCR activation, but not by TLR activation (Fig. 6C). Using rHRSV-Ch, we observed that viral infection of nBregs was associated with the highest frequencies of nBregs expression cell surface CX3CR1 relative to other stimuli. We found that an RSV ΔG mutant poorly infected nBregs (Fig. 6F-G) and was unable to induce IL-10 production (Fig. 6D), despite its ability to trigger BCR Igα phosphorylation (Fig. 6E). This indicates that G protein binding to CX3CR1 was necessary to induce IL-10 production. In the presence of the CX3CR1 ligand CX3CL1, RSV infection was strongly decreased, concomitant with the inhibition of the IL-10 secretion (Fig. 6H), indicating that CX3CL1 is blocking the interaction of the RSV G protein with CX3CR1, which is therefore essential for the induction of nBreg activity. Our results show that RSV, upon binding of surface Ig on nBregs, induces

the upregulation of CX3CR1 which, in turn, interacts with the G glycoprotein and favors viral entry and replication in Bregs. This two-step mechanism can explain the permissiveness of nBregs to RSV infection and the specific induction of IL-10 which does not occur with the other viruses tested.

RSV infects infant nBregs and nBregs are predictive of disease severity

Infants under 3 months of age who develop acute severe bronchiolitis because of RSV infection may require ventilator support and are at a much higher risk to develop recurrent wheezing up through their teenage years (Stein, 2009). This is often thought to be associated with Th2 responses. However, post-mortem analysis in fatal cases reveals heavy pulmonary infiltration of B cells, but not T cells, in the lung upon RSV infection (Reed et al., 2009). RSV remains in the respiratory tract and does not spread to the blood. IL-10 can be detected in the nasopharyngeal aspirates (NPA) of RSV-infected children (Bont et al., 2001) and is associated with post-bronchiolitis wheeze (Schuurhof et al., 2011). We therefore looked for the presence of nBregs in the NPA of hospitalized RSV-infected children who required respiratory assistance. In 6 out of the 13 patients, RSV-infected nBregs were found in NPA swabs, whereas 2 patients showed RSV-infected MN B cells, highlighting the preferential infection of nBregs in vivo. The frequency of nBregs correlated with the severity of the disease, as assessed by the duration of oxygen support and hospitalization in the ICU (Fig. 7A and Fig. S7). We also found a higher frequency of nBregs in the blood of RSV-infected patients suffering from acute bronchiolitis compared to non-infected children, and a positive correlation between the percentage of nBregs with the disease severity and the viral load, but not with the age of the patient or the pregnancy term (Fig. 7B-D and Fig. S7). In contrast to MN and IMT B cells, nBregs purified from the

blood of RSV-positive patients expressed *IL10* mRNA upon RSV exposure, but not *IL35*, *IL12A* and *EBI3*, subunits (Fig. 7E), indicating the capacity of nBreg activity to be activated following their recruitment at the site of infection.

In the neonatal blood, we identified emerging $CD4^+$ T cell effector memory (Tem) including $CXCR3^+$ IFN-γ producing Th1 cells (Zhang et al., 2014b). RSV-activated nBregs limited the development of neonatal Th1 responses in vitro (Fig. 2). We found a higher frequency of Tem cells, but not Treg cells, in the blood of RSV-infected children compared to RSV un-infected children. The percentage of Tem cells and $CXCR3^+$Tem cells negatively correlated with bronchiolitis severity, but not with the age of the patient or the pregnancy term (Fig. 7F-G and Fig. S7). Among the RSV-infected patients, the frequency of CXCR3+ Tem cells was significantly lower when nBregs were infected with RSV, as measured in the NPA (Fig. 7H). These findings indicate that RSV infection of nBregs may inhibit CXCR3+ Tem responses in patients to reduce viral clearance and to drive more severe lung disease.

Discussion

Using mass cytometry we identified nBregs, which are an age-dependent factor associated with the severity of RSV-induced acute bronchiolitis. RSV infects nBregs, through IgM recognition and induced CX3CR1 allowing viral interaction with the G glycoprotein. B cell interactions with pathogens without antigen specificity usually leads to B cell death and an impaired antibody responses (Nothelfer et al., 2015). The possibility of virus-mediated B-cell subversion in an antigen-specific manner has been proposed recently in the context of influenza specific-B cells (Dougan et al., 2013). Salmonella spp. Induces and/or activates Bregs in a TLR-dependent manner (Neves et al., 2010). In inflammatory situations, the CD40- and TLR-mediated

pathways are central in Breg activation (Mauri and Bosma, 2012). nBregs developed *in utero* cells and waned with age, likely reflecting a fetal-specific wave of B-cell ontogeny and selection. The polyreactive nature of the Ig repertoire of nBregs suggests that other pathogens may target nBregs. However, the BCR was not sufficient to activate nBregs as a second receptor was required in the context of RSV. The mechanism we propose involves the combined role of RSV G and F glycoproteins in hijacking the newborn immune system to impair viral clearance. The pre-fusion form of the F protein appears to be the critical target for virus neutralization (McLellan et al., 2013; McLellan et al., 2011). Of note, TLR4 was reported to interact with the F fusion protein of RSV in a CD14-dependent manner (Kurt-Jones et al., 2000). However human B cells do not express TLR4. The F fusion protein-BCR interaction that initiates nBreg activation enables G-CX3CR1-mediated infection, and the nBreg-IgM outcompeted and decreased the initial viral interaction and further infection. The IL-10 production by nBregs was mainly associated with the infection of the cell, although additional mechanisms such as TLR activation might contribute to the amplification of the antiinflammatory response.

In primary RSV infection in humans and mice, a type-I immune response including NK cells, Th1 cells, and cytotoxic T lymphocytes (CTLs) which act as important sources of IFN-γ, is essential for viral clearance (Openshaw and Chiu, 2013). An unbalanced and dysregulated T-cell response to HRSV limits viral clearance and is reported to cause immunopathology in the respiratory tract. Primary HRSV infection in newborn mice, during the critical neonatal window led to the generation of a type-II response, an enhanced airway inflammation, lymphocyte infiltration and eosinophilia upon re-infection at adulthood, whereas delayed age priming led to enhanced IFN-γ production and less severe symptoms during reinfection (Culley et al., 2002). Th2

pathology occurs upon secondary RSV infection, and is poorly associated with the primary infection. We found very few T cells in the NPA or effector memory Th1 cells in the blood and no detectable Th2 signature in the patients. Therefore, our *in vivo* and *in vitro* data support the role of RSV-activated nBregs in the control of IFN-γ Th1 cells and associated viral clearance.

It is unclear yet whether infected nBregs can reach the lymph nodes (LNs) and whether they directly influence directly Th1 priming. Human nBregs are related to neonatal B1a cells in terms of their regulatory properties (Sun et al., 2005; Zhang et al., 2007). Mouse B1a cells have been recently shown to be trans-infected by blood-borne retroviruses via LN macrophages (Sewald et al., 2015). In such a scenario, RSV might reach nBregs in the lung draining LN via myeloid cells. Such innate B cells procduce natural antibodies with polyreactive properties. The hallmark of the human innate B cells is the expression of CD27, a marker corresponding to memory cells. Carsetti and colleagues defined “IgM memory cells” in the blood as cells that are IgM+IgD+CD22+CD27+ (Kruetzmann et al., 2003), splenic MZBs are defined as IgMhiIgDlowCD23−CD21+CD1c+CD27+ (Weller et al., 2008) and B1 cell candidate are IgM+IgD+CD43+CD27+ B cells (Griffin et al., 2011). This IgM memory/MZB compartment develops following birth, possibly in response to the gut microbiota. The human B1 cells would represent a minority in neonatal blood but could account for 40 % of all CD27+ memory B cells. This latter point raised some controversies about the phenotype of these cells, that would include T cell or monocyte contaminants (Descatoire et al. 2011 ; Perez-Andres, 2011). A small fraction of human B1 cell express CD5, which is the hallmark of nBreg, and do not hhave any repertoire bias in ciontrast to nBreg. The cyTOF approach we had clearly eliminate the possibility of other cell lineage contamination. to CD5 and CD27 expression. The “human B1 cells”

have been proposed to be pre-plasmablasts because they produce IgM, IgG and IgA, and we showed nBregs to be free of any IgG or IgA positive cells. In addition, nBreg quickly wanes with age whereas human B1 cell population would develop. This age depedency of nBreg might explain their contribution to RSV disease which becomes asymptomatic later in age. We also showed that canonical adult memory B cells can be slightly infected by the RSV. Therefore it remains to be determined whether they correspond to a small fraction of RSV specific B cells and whether their infection could play a role in the susecptibilty to the infection later in life, in the elderly poplulation.

In addition to lung epithelial cells, nBregs represent a newly described target cell for RSV and a biomarker for the severity of acute bronchiolitis. A recent study that defined biomarkers in bronchiolitis using whole blood RNA profiling, highlighted an overexpression of neutrophil and interferon genes as well as suppression of B- and T-cell genes in children of less than 6 months (Mejias et al., 2013). The increased number of nBregs observed in the blood emphasizes how carefully B cell signatures need to be interpreted. Therefore, the appropriate complex signal deconvolution of whole blood signatures needs to take into account age-specific immune characteristics. If confirmed in the NPA, the “RSV-nBreg” signature that we defined may serve as a molecular biomarker of disease severity. Future work will determine whether the high frequency of nBregs is a consequence or a cause of the disease. In future investigations, large cohorts are needed to determine whether nBreg is a host risk factor that might predispose individuals to RSV-induced bronchiolitis. nBreg activity may constitute an early-life host response that favors microbial pathogenesis and may represent a target for the treatment of low respiratory tract viral infections and their pathological consequences later in life.

Experimental procedures

Blood.

Buffy coats were obtained from adult donors by the Etablissements Français du Sang (France). Heparinized cord blood samples from healthy neonates collected by the Thérapie Cellulaire of Hopital Saint-Louis (France). Written consent was obtained from the mothers. This study was conducted with the approval of the Ethics Committee of Institut Pasteur in agreement with the principles of the Declaration of Helsinki. For FACS analysis of infant B cells, we used blood samples from children from birth to 5 years of age that were admitted to the Hopital Erasme laboratory (Brussels, Belgium) for routine analysis of the common hematological parameters between March 2012 and June 2012. The final protocol of this study was approved by the Ethics Committee of Erasme Hospital, allowing us to test residual blood samples.

Cohort of patients with acute bronchiolitis.

46 infants admitted to the NICU of the Bicêtre Hospital for severe bronchiolitis were recruited. Infants being prophylactically treated with Palivizumab were excluded. After signed informed consent from the legal representatives of the children, 1 mL of blood in EDTA tubes (Sarstedt) and nasopharyngeal aspirates were obtained and stored at 4°C and at -80°C. Samples were processed within 12 h. Diagnosis of viral bronchiolitis was confirmed using immunochromatography for RSV (Alere BinaxNow RSV, Alere) and respiratory virus Q-PCR techniques (either Simplexa Flu A/B &

RSV Direct, Focus Diagnostics; or Argene Respiratory Multi Well System MWS r-gene range, Biomerieux). The study was approved by the local IRB (Pasteur Institute CoRC, no 2013-14) and the French Ministry of Research (no. 13.644). Details of the demographic and diagnostic data are detailed in the supplementary experimental procedures.

Culture Medium and Reagents.

Complete medium consisted of RPMI-1640 supplemented with 10% fetal calf serum (ICN Biomedicals), $5x10^{-5}$ M of 2-ME (Sigma), and antibiotics (Gibco BRL). R848 was purchased from InvivoGen. Human Influenza Virus A/PR/8/34 (IAV) was purchased from Charles River. Measles virus (MV, strain Schwarz) were amplified and titrated using Vero cells. Human coronavirus (HCoV-229E), Herpes simplex virus 1 (HSV, strain KOS), Human immunodeficiency virus (HIV) were used. Human T-lymphotropic virus (HTLV-1) was produced with Mt2 cell supernatants (kindly provided by MA Thoulouze). Epstein-Barr virus (EBV) was generated using B95.8 cell line. Recombinant human BAFF, IL-2 and IL-12 were purchased from Peprotech. CX3CL1 was from R&D Systems.

HRSV strains and mutants

Human respiratory syncytial virus A (HRSV-A Long, kindly provided by F. Freymuth) was amplified and titrated on HEp-2 cells. Recombinant Human RSV (rHRSV-A) and recombinant Human RSV-Cherry (rHRSV-Ch) were previously described (Rameix-Welti et al., 2014). The procedures to generate the rHRSV-ΔG-Cherry and rHRSV-ΔSH are described in the supplementary info.

RSV specific ELISA.

Maxisorp plates (NUNC) were coated with HRSV-A, or ΔSH and ΔG mutants or their WT counterparts described above at 4 °C overnight. Following blocking of the plates with 1% BSA in PBS at 37 °C for 1 h, IgM from CpG-stimulated cord blood B cell subsets were added to the plates for 1 h at room temperature. After washing, horseradish peroxidase (HRP) conjugated to goat anti-human IgM (Southern Biotech) with a TMB substrate was used. Optical densities (OD) were measured at 450 nm.

Mass cytometry.

The antibodies were labeled 100 µg at a time according to the manufacturer's instruction with heavy metal-preloaded maleimide-coupled MAXPAR chelating polymers. Purified antibodies were purchased from Miltenyi. CBMC were stained with these reagents, DNA content stained by an iridium-191/193 interchelator was used to identify individual cells, and by exclusion of a live-dead viability stain. Data were acquired using a CyTOF2 instrument (Fluidigm) and analyzed using vISNE algorithm on Cytobank (Fluidigm). Antibody clones used are detailed in the supplementary experimental procedures.

Cell purification and culture

CBMCs or PBMCs from child patients or adults were isolated using Lymphoprep (Axis-Shield). B cells were positively enriched from CBMCs or PBMCs by using anti-CD19 magnetic beads with AutoMACS (Miltenyi Biotec). To recover the blood B cell subsets, the cells were sorted based on surface CD10 and CD5 markers to obtain $CD10^{+}CD5^{+}$ (IMT), $CD10^{-}CD5^{hi}$ (nBreg) and $CD10^{-}CD5^{-}$ (MN) B cell subsets using a FACS Aria 3 (BD). Cells sorted by AutoMACS and FACS were routinely >95% and

97-99% pure, respectively. B cells were stimulated with indicated compounds or viruses for 48 hours (MOI=2.5). For co-culture assay, mycoplasma-free HEp-2 cells were incubated for 2h at 37°C with rHRSV-Ch, supernatants were then discarded. 24 h later, cells were washed twice with PBS (1x), and purified nBregs, MN, or IMT B cells were added to the infected HEp2 cells for 48 h. Alternatively, cells were cultured with human BAFF (200 ng/ml), CpGB 1826 (5 µg/ml), and IL-2 (10 ng/ml). The supernatants were measured for IL10 by ELISA (eBioscience). To monitor infection of cells, mCherry fluorescence was detected either by LSR Fortessa FACS (BD) or IncucyteZoom (Essen Bioscience) for live cell imaging. Antibodies used for FACS are described in the supplementary experimental procedures.

Nasopharyngeal aspirate cells isolation.

Nasopharyngeal aspirates (NPA) were maintained on ice and processed within 24 h. The samples were repeatedly washed with PBS with 5% FCS and centrifuged until no visible mucus clumps remained in the solution. The samples were then filtered using a Falcon 100-µm filter (Miltenyi Biotech). For nasal wash cell staining and isolation, filtered NPA cells were incubated with antibodies for 20 min.

B cell repertoire analysis.

We characterized the IgM repertoire at the molecular level in various B-cell subsets from cord blood and the details can be found in the supplementary information.

Microarray analysis.

$5x10^3$ negatively-enriched cord blood B cells were FACS-sorted as nBregs ($CD19^+CD5^+CD10^-CD3^-$), and stimulated for 6 h with 10 µg/ml F(ab')2 goat anti-

human IgM, R848 (1µg/ml), HRSV-A (MOI=5) or IAV (MOI=4000HA/ml). The gene expression profiles were measured by Miltenyi Biotec using an Agilent DNA chip. We used the Agilent 60-mer Whole Human Genome Oligo Microarray containing approximately 44 K genes and gene candidates. Raw expression files and details can be accessed at the following link: http://www.ncbi.nlm.nih.gov/geo/query/acc.cgi?token=orifscmydxsxvav&acc=GSE78847. Output data files were further analyzed using the Rosetta Resolver gene expression data analysis system. Microarrays Agilent files were processed, background corrected, and normalized using the quantile method with R and package Limma. Genes were averaged using ProbeID, and GeneName and transcripts were filtered using the refseq mRNA database. Principal component analyses on most differentially expressed genes, heatmaps and hierarchical clustering were performed using Qlucore Omics Explorer 3.1.

Gene expression.

10^3 blood B cells stimulated or not with HRSV for 24h, were then analysed using appropriate primers for expression of *EBI3 (*CCCTTCCCAGAGATCTTCTCAC ; CAGCCCTGAGGATGAAGGAC*), IL10 (*CCGTGGAGCAGGTGAAGAA ; GTCAAACTCACTCATGGCTTTGTA*), and IL12A (*CACAGTGGAGGCCTGTTTA ; *TCTGGAATTTAGGCAACTCTCA*RNA*)* on a Biomark System (Fluidigm).

Intracellular staining assay.

$CD19^+$ B cell fraction was stained with surface markers (CD20, CD10, CD5 and CD3) and live/dead-Blue to identify viable B cell subsets. Cells were stimulated for 30 min

with 10 µg/ml F(ab')2 goat anti-human IgM, R848 (1µg/ml), HRSV-A (MOI=1/10) or IAV (MOI=4000HA/ml). Cells were then directly fixed and permeabilized using BD Cytofix/Cytoperm™ solution by following the manufacturer's instructions (eBioscience) and then subjected to intracellular phospho-CD79a detection.

T cell differentiation in vitro.

$5x10^4$ purified cord blood naïve $CD4^+$ T cells activated with anti-CD3/CD28 beads in Th0 (no cytokine added) or Th1 (with 10 ng/ml of IL-12) conditions were co-cultured with $5x10^4$ syngeneic B activated with HRSV. Alternatively, purified cord blood pDCs were stimulated with HRSV-A in the presence of nBregs for 48 h. Activated pDCs were sorted again by gating on CD123hiCD20- cells on FACSAria II. 10^4 activated pDCs were co-cultured with $5x10^4$ purified allogeneic cord blood naïve $CD4^+$ T cells. Five-six days later, differentiated T cells were restimulated with 50 ng/ml PMA, 1 µg/ml Ionomycin and GolgiPlug (BD) to detect intracellular cytokines (IL-2, IFN-γ, IL-13, IL-17, IL-22 and TNF-α), Alternatively, secreted IFN-γ, IL-13 and IL-17 were detected by ELISA with a specific kit (eBiosciences).

ELISPOT

nBregs were stimulated or not with HRSV-A for 24h. IL10 secreting nBregs were enriched using IL-10 cytokine secretion assay according to the manufacturer's protocol (Milteny Biotec). Enriched cells were then FACS sorted for IL-10-positive cells and used for human fluoroSpot IgM according to the manufacturer's protocol (Mabtech). Alternatively, IgM secreting cells were also analysed with an HRP-based ELISPOT assay (Mabtech).

Statistical analysis. Unpaired *t* tests were done in comparison of two groups (data are presented as the mean value ± SD). Paired *t* tests were also used to take into account donor to donor variation. ANOVA tests were used when comparing three groups or more. Spearman tests were used for correlations. *P* values <0.05 were considered statistically significant.

Supplementary information :

7 supplementary Figures with legends, and supplementary experimental procedures.

References

Amir el, A.D., Davis, K.L., Tadmor, M.D., Simonds, E.F., Levine, J.H., Bendall, S.C., Shenfeld, D.K., Krishnaswamy, S., Nolan, G.P., and Pe'er, D. (2013). viSNE enables visualization of high dimensional single-cell data and reveals phenotypic heterogeneity of leukemia. Nature Biotech *31*, 545-552.

Blair, P.A., Noreña, L.Y., Flores-Borja, F., Rawlings, D.J., Isenberg, D.A., Ehrenstein, M.R., and Mauri, C. (2010). CD19(+)CD24(hi)CD38(hi) B Cells Exhibit Regulatory Capacity in Healthy Individuals but Are Functionally Impaired in Systemic Lupus Erythematosus Patients. Immunity *32*, 129-140.

Bont, L., Heijnen, C.J., Kavelaars, A., van Aalderen, W.M., Brus, F., Draaisma, J.M., Pekelharing-Berghuis, M., van Diemen-Steenvoorde, R.A., and Kimpen, J.L. (2001). Local interferon-gamma levels during respiratory syncytial virus lower respiratory tract infection are associated with disease severity. J Infect Dis *184*, 355-358.

Castro, M., Schweiger, T., Yin-Declue, H., Ramkumar, T.P., Christie, C., Zheng, J., Cohen, R., Schechtman, K.B., Strunk, R., and Bacharier, L.B. (2008). Cytokine response after severe respiratory syncytial virus bronchiolitis in early life. J Allergy Clin Immunol *122*, 726-733 e723.

Culley, F.J., Pollott, J., and Openshaw, P.J. (2002). Age at first viral infection determines the pattern of T cell-mediated disease during reinfection in adulthood. J Exp Med *196*, 1381-1386.

Descatoire, M., Weill, J.C., Reynaud, C.A., and Weller, S. (2011). A human equivalent of mouse B-1 cells? J Exp Med 208, 2563-2564; author reply 2566-2569.

Dougan, S.K., Ashour, J., Karssemeijer, R.A., Popp, M.W., Avalos, A.M., Barisa, M., Altenburg, A.F., Ingram, J.R., Cragnolini, J.J., Guo, C., *et al.* (2013). Antigen-specific B-cell receptor sensitizes B cells to infection by influenza virus. Nature *503*, 406-409.

Fillatreau, S., Sweenie, C.H., McGeachy, M.J., Gray, D., and Anderton, S.M. (2002). B cells regulate autoimmunity by provision of IL-10. Nat Immunol *3*, 944-950.

Griffin, D.O., Holodick, N.E., and Rothstein, T.L. (2011). Human B1 cells in umbilical cord and adult peripheral blood express the novel phenotype CD20+CD27+CD43+CD70-. J Exp Med *208*, 67-80.

Kruetzmann, S., Rosado, M.M., Weber, H., Germing, U., Tournilhac, O., Peter, H.H., Berner, R., Peters, A., Boehm, T., Plebani, A., et al. (2003). Human immunoglobulin M memory B cells controlling Streptococcus pneumoniae infections are generated in the spleen. J Exp Med 197, 939-945.

Kurt-Jones, E.A., Popova, L., Kwinn, L., Haynes, L.M., Jones, L.P., Tripp, R.A., Walsh, E.E., Freeman, M.W., Golenbock, D.T., Anderson, L.J., *et al.* (2000). Pattern recognition receptors TLR4 and CD14 mediate response to respiratory syncytial virus. Nat Immunol *1*, 398-401.

Lemoine, S., Morva, A., Youinou, P., and Jamin, C. (2011). Human T cells induce their own regulation through activation of B cells. J Autoimmun *36*, 228-238.

Matsushita, T., Yanaba, K., Bouaziz, J.-D., Fujimoto, M., and Tedder, T.F. (2008). Regulatory B cells inhibit EAE initiation in mice while other B cells promote disease progression. J Clin Invest *118*, 3420-3430.

Mauri, C., and Bosma, A. (2012). Immune regulatory function of B cells. Ann Rev Immunol *30*, 221-241.

Mauri, C., Gray, D., Mushtaq, N., and Londei, M. (2003). Prevention of arthritis by interleukin 10-producing B cells. J Exp Med *197*, 489-501.

McLellan, J.S., Chen, M., Leung, S., Graepel, K.W., Du, X., Yang, Y., Zhou, T., Baxa, U., Yasuda, E., Beaumont, T., *et al.* (2013). Structure of RSV fusion glycoprotein trimer bound to a prefusion-specific neutralizing antibody. Science *340*, 1113-1117.

McLellan, J.S., Yang, Y., Graham, B.S., and Kwong, P.D. (2011). Structure of respiratory syncytial virus fusion glycoprotein in the postfusion conformation reveals preservation of neutralizing epitopes. J Virol *85*, 7788-7796.
Mejias, A., Dimo, B., Suarez, N.M., Garcia, C., Suarez-Arrabal, M.C., Jartti, T., Blankenship, D., Jordan-Villegas, A., Ardura, M.I., Xu, Z., *et al.* (2013). Whole blood gene expression profiles to assess pathogenesis and disease severity in infants with respiratory syncytial virus infection. PLoS Med *10*, e1001549.
Menon, M., Blair, P.A., Isenberg, D.A., and Mauri, C. (2016). A Regulatory Feedback between Plasmacytoid Dendritic Cells and Regulatory B Cells Is Aberrant in Systemic Lupus Erythematosus. Immunity *44*, 683-697.
Neves, P., Lampropoulou, V., Calderon-Gomez, E., Roch, T., Stervbo, U., Shen, P., Kühl, A.A., Loddenkemper, C., Haury, M., Nedospasov, S.A., *et al.* (2010). Signaling via the MyD88 Adaptor Protein in B Cells Suppresses Protective Immunity during Salmonella typhimurium Infection. Immunity *33*, 777-790.
Nothelfer, K., Sansonetti, P.J., and Phalipon, A. (2015). Pathogen manipulation of B cells: the best defence is a good offence. Nature Rev Microbiol *13*, 173-184.
Perez-Andres, M., Grosserichter-Wagener, C., Teodosio, C., van Dongen, J.J., Orfao, A., and van Zelm, M.C. (2011). The nature of circulating CD27+CD43+ B cells. J Exp Med 208, 2565-2566; author reply 2566-2569.
O'Garra, A., Chang, R., Go, N., Hastings, R., Haughton, G., and Howard, M. (1992). Ly-1 B (B-1) cells are the main source of B cell-derived interleukin 10. Eur J Immunol *22*, 711-717.
Openshaw, P.J., and Chiu, C. (2013). Protective and dysregulated T cell immunity in RSV infection. Curr Opin Vvirol *3*, 468-474.
Prabhudas, M., Adkins, B., Gans, H., King, C., Levy, O., Ramilo, O., and Siegrist, C.-A. (2011). Challenges in infant immunity: implications for responses to infection and vaccines. Nat Immunol *12*, 189-194.
Rameix-Welti, M.A., Le Goffic, R., Herve, P.L., Sourimant, J., Remot, A., Riffault, S., Yu, Q., Galloux, M., Gault, E., and Eleouet, J.F. (2014). Visualizing the replication of respiratory syncytial virus in cells and in living mice. Nat Comm *5*, 5104.
Reed, J.L., Welliver, T.P., Sims, G.P., Mckinney, L., Velozo, L., Avendano, L., Hintz, K., Luma, J., Coyle, A.J., and Welliver, R.C. (2009). Innate immune signals modulate antiviral and polyreactive antibody responses during severe respiratory syncytial virus infection. J Infect Dis *199*, 1128-1138.
Schuurhof, A., Janssen, R., de Groot, H., Hodemaekers, H.M., de Klerk, A., Kimpen, J.L., and Bont, L. (2011). Local interleukin-10 production during respiratory syncytial virus bronchiolitis is associated with post-bronchiolitis wheeze. Respir Res *12*, 121.
Sewald, X., Ladinsky, M.S., Uchil, P.D., Beloor, J., Pi, R., Herrmann, C., Motamedi, N., Murooka, T.T., Brehm, M.A., Greiner, D.L., *et al.* (2015). Retroviruses use CD169-mediated trans-infection of permissive lymphocytes to establish infection. Science *350*, 563-7.
Shen, P., Roch, T., Lampropoulou, V., O'Connor, R.A., Stervbo, U., Hilgenberg, E., Ries, S., Dang, V.D., Jaimes, Y., Daridon, C., *et al.* (2014). IL-35-producing B cells are critical regulators of immunity during autoimmune and infectious diseases. Nature *507*, 366-370.
Siegrist, C.A. (2001). Neonatal and early life vaccinology. Vaccine *19*, 3331-3346.
Smyth, R.L., and Openshaw, P.J. (2006). Bronchiolitis. Lancet *368*, 312-322.
Stein, R.T. (2009). Long-term airway morbidity following viral LRTI in early infancy: recurrent wheezing or asthma? Paediatr Respir Rev *10*, 29-31.
Sun, C., Deriaud, E., Leclerc, C., and Lo-Man, R. (2005). Upon TLR9 signaling, CD5(+) B cells control the IL-12-dependent Th1-priming capacity of neonatal DCs. Immunity *22*, 467-477.

Tayyari, F., Marchant, D., Moraes, T.J., Duan, W., Mastrangelo, P., and Hegele, R.G. (2011). Identification of nucleolin as a cellular receptor for human respiratory syncytial virus. Nat Med *17*, 1132.
Teng, M.N., Whitehead, S.S., and Collins, P.L. (2001). Contribution of the respiratory syncytial virus G glycoprotein and its secreted and membrane-bound forms to virus replication in vitro and in vivo. Virology *289*, 283-296.
Tripp, R.A., Jones, L.P., Haynes, L.M., Zheng, H., Murphy, P.M., and Anderson, L.J. (2001). CX3C chemokine mimicry by respiratory syncytial virus G glycoprotein. Nat Immunol *2*, 732-738.
Weill, J.-C., Weller, S., and Reynaud, C.-A. (2009). Human marginal zone B cells. Annu Rev Immunol *27*, 267-285.
Weller, S., Mamani-Matsuda, M., Picard, C., Cordier, C., Lecoeuche, D., Gauthier, F., Weill, J.-C., and Reynaud, C.-A. (2008). Somatic diversification in the absence of antigen-driven responses is the hallmark of the IgM+ IgD+ CD27+ B cell repertoire in infants. J Exp Med *205*, 1331-1342.
Welliver, T.P., Garofalo, R.P., Hosakote, Y., Hintz, K.H., Avendano, L., Sanchez, K., Velozo, L., Jafri, H., Chavez-Bueno, S., Ogra, P.L., *et al.* (2007). Severe human lower respiratory tract illness caused by respiratory syncytial virus and influenza virus is characterized by the absence of pulmonary cytotoxic lymphocyte responses. J Infect Dis *195*, 1126-1136.
Zhang, X., Casartelli, N., Lemoine, S., Mozeleski, B., Azria, E., Le Ray, C., Schwartz, O., Launay, O., Leclerc, C., and Lo-Man, R. (2014a). Plasmacytoid dendritic cells engagement by influenza vaccine as a surrogate strategy for driving T-helper type 1 responses in human neonatal settings. J Infect Dis *210*, 424-434.
Zhang, X., Deriaud, E., Jiao, X., Braun, D., Leclerc, C., and Lo-Man, R. (2007). Type I interferons protect neonates from acute inflammation through interleukin 10-producing B cells. J Exp Med *204*, 1107-1118.
Zhang, X., Mozeleski, B., Lemoine, S., Deriaud, E., Lim, A., Zhivaki, D., Azria, E., Le Ray, C., Roguet, G., Launay, O., *et al.* (2014b). CD4 T cells with effector memory phenotype and function develop in the sterile environment of the fetus. Sci Transl Med *6*, 238ra272.

ACKNOWLEDGEMENTS

We are very grateful to T. Domet (Therapie Cellulaire, Hopital Saint-Louis) for the cord blood sample collection and M. Lucas-Hourani for some viral preparation. We thank F. Huetz for helpful discussion about B lymphocytes. This work was supported by an ANR grant (ANR 13-BSV3-0016) and by the Fondation pour la Recherche Médicale (grant N° DEQ20120323719). This study also received funding from the French Government's Investissement d'Avenir program, Laboratoire d'Excellence "Integrative Biology of Emerging Infectious Diseases" (grant n°ANR-10-LABX-62-IBEID). X.Z. and S.L. were supported by ANR and by the European Commission FP7 ADITEC program (HEALTH-F4-2011-280873). X.Z. was also partially supported by the Major Basic Research Project of Shanghai Science and Technology Commission (No. 13JC1405600); National Natural Science Foundation of China (31270961, 31470879); Interdisciplinary Innovation Team and External Cooperation Program (No. GJHZ201312), Chinese Academy of Sciences". D.Z. was supported by DIM Malinf of Region IdF. Work in the O.S. lab is also supported by ANRS, Sidaction and Fondation Areva. We acknowledge the Center for Human Immunology at Institut Pasteur for support in conducting these studies.

Author contribution

DZ designed and performed research. SL performed bioinformatics analysis of the transcriptomics data. AL completed the repertoire study. AM, LS, NC, ED, JF, BB, MRL, JM, BL, VL performed experiments and analyzed data. AL, POV, MARW, PLH, DD, JFE, OS, FP, FM, HM and XZ provided reagents and contributed to experimental design. XZ, PT and RLM designed and supervised the project. DZ, POV, XZ, SR, JFE, HM and PT critically revised the manuscript. RLM wrote the manuscript.

The authors have no conflicting financial interest.

Legends to Figures

Figure 1: Identification of phenotypic of new population of regulatory B cells in the human neonate (nBregs).

(A-B) CyTOF analysis of cord blood CD19+ B cells within CMBCs for lineage and B cell markers. (A) Data analysis using viSNE based on 19 markers delineating phenotype CD10-CD5- (1), CD10+CD5+ (2) and CD10-CD5+ (3). (B) Heatmap analysis for data corresponding to the fold change expression of indicated markers for each subset as compared to the whole CD19+CD20+ B cell population (C) Cord blood B cell subsets were FACS sorted as, CD10-CD5- (MN; blue), CD10+CD5+ (IMT; green) and CD10-CD5+ (nBreg; red). 10^5 cord blood B cell subsets were stimulated with HRSV-A (MOI=2.5) and IL-10 production was measured at 48h by ELISA (n=3). Results are expressed as the means +/- SD. (D) Percentage of the nBreg subset among the total B cells circulating in the blood during different developmental stages and ages. *p<0.05, **p<0.01. (E) X and Y chromosome FISH staining of nBreg cells isolated from cord blood of a male baby. Bar chart indicates the number of nuclei associated with XY or XX staining.

Figure 2 : nBregs regulate TH cell polarization directly or indirectly via pDCs.

(A-C) Neonatal naive CD4+ T cells were activated by anti-CD3 + anti-CD28 and cultured with 10 ng/ml IL-12 (Th1) or without (Th0), alone or in co-culture with HRSV-activated nBregs for 6 days. (A) FACS plots and (B) mean frequencies of TNF-α, IL-2, IFN-γ, IL-13, IL-17 or IL-22 secreting cells, as determined by intracellular staining for 5 donors (Anova test). (C) Quantification of IFN□γ□in the supernatants of the same co-cultures, as determined □□□□□□□□ (n=4 donors; paired t-test was used

for comparison). (D-F) Neonatal pDCs were stimulated with HRSV-A either alone or in co-culture with nBregs in the presence of neutralizing anti-IL-10 or control antibody (Ctrl) for 48 h. pDCs were FACS purified again before being used in TH differentiation assay. (D-E) Intracellular IFN-γ, IL-4, IL-17 and IL-22 expression was analyzed by FACS and (F) secreted IFN-γ analyzed in the supernatants by ELISA. (D-F) Results are representatives of 3 experiments. Results are expressed as the means ± SD. *p<0.05, **p<0.01, ** p<0.001 and NS for non significant.

Figure 3: nBregs are preferentially infected by RSV.

(A-C) 10^5 cord blood nBregs were FACS sorted and left untreated (0 h) or exposed to HRSV-A or to rHRSV-Ch (MOI=2.5). (A) Representative plot of *IL10* gene expression, as measured by qRT-PCR at 0h, 6h and 24h. (B) 10^5 B cell subsets were FACS sorted as nBreg, MN or IMT and stimulated with rHRSV-Ch. mCherry expression was assessed by fluorescent microscopy at 48h post-infection (left panel) or by monitoring the red object count (R.O.C) through live imaging (right panel). Results are representitative of 3-5 independent experiments. (C) Representative FACS plot for intra-cellular IL-10 expression at 48h post-infection as compared to untreated cells (No stimulus). (D) The frequency of $IL10^+$ nBreg cells among rHRSV-Ch-positive or -negative nBregs(n=3). Unpaired t-test was used for comparison. (E) IL-10 production following nBreg exposure to live or UV-treated HRSV-mCherry was measured at 48h by ELISA (n=5). Paired *t* test was also used to compare the three conditions. (F-G) HEp-2 cells were infected with rHRSV-Ch (MOI=0.1) then cocultured with B cell subsets (F) The percentage of rHRSV-Ch^+ B cells in co-culture with HEp-2 cells is shown by FACS at 48 h post coculture (n=3). ANOVA test was used to compare the three groups. (G) IL-10 production was measured by ELISA

(n=3) and unpaired t-test was used for comparison. (H) nBregs were stimulated or not with HRSV-A for 24h. IL10+ nBregs were then enriched using IL-10 enrichement beads, then FACS sorted IL10+ nBregs were used for fluorescent IgM ELISPOT. Left panel is a representative FACS plot following IL-10 enrichement and sorting purity. Right panel indicate the frequency of IgM+ cells. Results are expressed as the means ± SD of triplicates. *p<0.05, **p<0.01, ***p<0.001.

Figure 4: RSV activates the BCR pathway

5.10^3 Cord blood nBregs were FACS-sorted as CD19+CD5+CD10- B cells, and stimulated for 6h with aIgM, R848, HRSV-A, IAV or left unstimulated. Gene expression profiles were compared by microarray analysis for 3 independent donors. (A) PCA and (B) heatmap of hierarchical clustering corresponding to the indicated stimulus (p=0.0049 and q=0.067; 745 genes). (C) The list of differentially expressed genes (p<0.05) was processed using the Ingenuity pathway analysis software. The list was then manually curated to remove pathways irrelevant to B cell biology. Canonical pathways were considered significant for p<0.05 (red line). (D-E) nBregs were activated for 30 min. with aIgM, R848, HRSV-A, IAV or left unstimulated. Phopshorylation of CD79a was assessed intracellularly by FACS. (D) Representative FACS plots and (E) means ± SD of 3 experiments are shown *p<0.05, **p<0.01, ***p<0.001.

Figure 5 : Ig from nBregs recognize RSV and display a biased repertoire

(A-C) IgM from three donors (d#1, d#2 and d#3) were produced by nBregs and MN neonatal B cell subsets following their stimulation with CpG B (1826) for 4 days and then were tested by ELISA for recognition of WT HRSV-A (left panel, IgM 4µg/ml), HRSV-F protein or HIV-1 gp140 protein (right panel; serial dilutions of IgM). Results

are expressed as optical density measured at 450 nm (O.D. 450 nm). (B) IgM (100 ng/ml) from nBregs were tested by ELISA for HRSV-A recognition in the presence of various doses of anti-F Palivizumab IgG Ab. (C) rHRSV-Ch was pre-incubated with nBreg-, MN- or IMT-derived IgM (50 ng/ml) for 1h prior infection. RSV infection was assessed by monitoring mCherry expression by fluorescent live microscopy. Histogram plot shows the frequency of inhibition at 48h post-infection with rHRSV-Ch/IgM mixes as compared to free rHRSV-Ch. Results are expressed as means ± SD of triplicates, and are representative of 2 experiments. (D-F) B cell subsets were subjected to Ig repertoire analysis of the IgM heavy chain (n=5-6 donors). (D) The mean CDR3 lengths was analyzed for the different IGHV, and a profile comparison is shown for IGHV3. (E) The frequencies of different IGHJ usage among V3a (V3-15, 49, 72, 73) subfamily were determined. (F) For IGH3 subfamily 3a family, 165 clones from MN and 185 clones from nBregs were sequenced to determine IGHJ/IGHD junctions. Among IGHJ4, the number for the different D gene usage is indicated (n=74 for MN, and n=84 for nBregs).

Figure 6 : HRSV infects nBreg cells via CX3CR1-G protein interaction

(A-C) FACS analysis of CX3CR1 expression in nBregs. (A) Representative FACS plot of freshly isolated nBregs (MFI: 193 for Ab ctrl, and 237 for CX3CR1 Ab) as compared to $CD14^+$ monocytes (MFI: 9971). (B) nBreg cells were infected with HRSV-A (MOI=2.5) for 48h. MFI are shown for CX3CR1 Ab as compared to isotype control. Results are expressed means ± SD of duplicates from 3 donors. (C) nBreg cells were stimulated with R848, agM or HRSV-A (MOI=2.5) for 48h and their CX3CR1 expression was assessed by FACS. Results are expressed as means ± SD of duplicates from 2 independent experiments. nBregs were infected for 48h with WT

or ΔG strains of rHRSV-Ch (MOI=2.5). (D) IL-10 production was measured by ELISA. Results are expressed as means ± SD of 4 independent experiments. (E) Phopshorylation of CD79a was assessed intracellularly by FACS in nBregs after 30 min. of exposure to ΔG RSV or WT RSV. Results are expressed means ± SD of triplicates, and are representative of 3 experiments. (F) Representative FACS plot (left panel) of nBregs infection with ΔG RSV or WT RSV, as compared to non-infected cells (none). Histogram plot shows the percentage of infected nBregs, as measured by FACS as % of mCherry+ cells (right panel) and is representative of 3 independent experiments. (G) Viral replication measured through the detection of the mCherry fluorescence for 48h with ΔG as compared to WT counterpart. Results are expressed as means ± SD of triplicates and are represent 3 independent experiments. (G) nBreg cells were cultured on CX3CL1-coated plates and infected with rHRSV-Ch (MOI=2.5). The percentage of infected nBregs and IL-10 secretion were measured at 48h. Results are expressed as means +/- SD and represent three independent experiments. Unpaired t-test were used for comparison. Results are expressed as the means +/- SD. **p<0.01, ***p<0.001, ****p<0.0001.

Figure 7 : nBregs are infected by RSV in patients and predict the severity of acute bronchiolitis.

(A) CD20+ B cells in nasopharyngeal aspirates (NPA) collected from RSV-positive patients (n=13) at the first day of hospital admission were analyzed and purified by FACS as nBregs and MN B cell subsets based on CD5 and CD10 expression. Heatmap shows sorted cell subsets analyzed for RSV nucleoprotein gene (RSV N) expression by qRT-PCR. Correlation plots (right panel) of nBreg cells frequency in the NPA with the duration of oxygen supply. (B) Frequency of B cells subsets in the

blood of RSV-positive (RSV^{pos}; n= 18) and negative (RSV^{neg}; n=10) patients. (C) Correlation plot of B cell subsets % in the blood of RSV^{pos} patients (n=18) with the duration of oxygen supply. (D) Correlation plot of blood nBreg cells frequency with RSV load in the corresponding NPA of RSV^{pos} patients (n=13). (E) nBreg, MN and IMT B cells were sorted from the blood of RSV^{pos} patients (n=7) and stimulated or not with HRSV for 24h. *IL10, EBI3 and IL12* gene expression for was analyzed by qRT-PCR and normalized to housekeeping genes. (F) CD4+ T cells were analyzed by FACS for Tregs and Tems, as shown in the blood of RSV-positive and (RSV^{pos}; n= 13) and negative (RSV^{neg}; n=7) patients. (G) Correlation plots of blood Tem and CXCR3+ Tem frequencies with the duration of oxygen supplementation (n=13). (H) Representative FACS analysis plot of blood CXCR3+ and CCR6+ Tem cells in patients whose nBreg cells were found infected or not in the NPA of panel (A). Histograms represent the frequency of CXCR3+ Tem cells in the blood (left histogram) and nBregs *IL-10* gene expression in the NPA (right histogram) from patients corresponding to infected nBreg (RSV^{pos}; n=3) or non infected nBreg (RSV^{neg}; n=3) Results are expressed as the means +/- SD. *p<0.05, **p<0.01, ***p<0.001. ns for non significant.

Figure 1

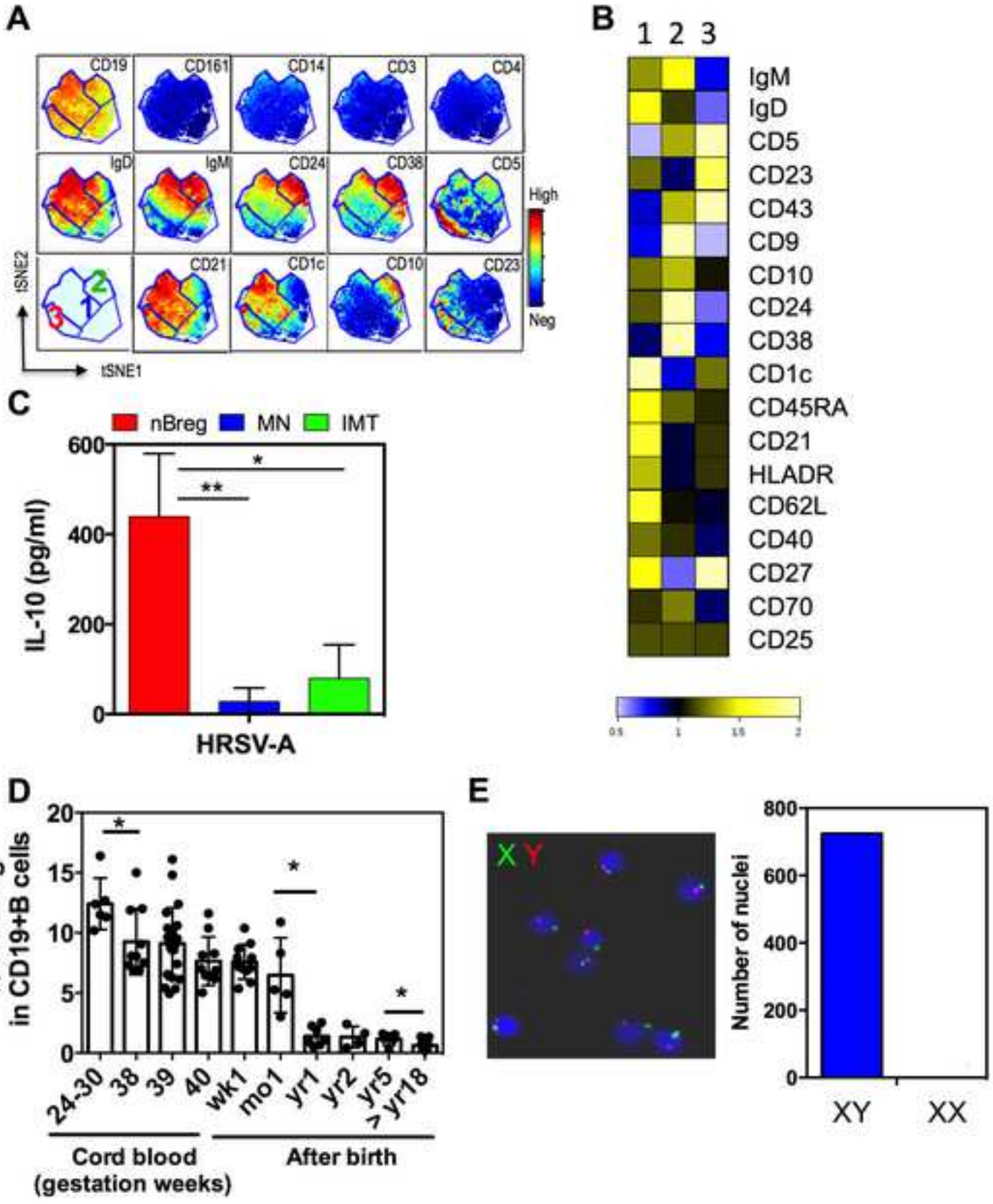

Figure 2

Click here to download Figure Fig2_R4.jpg

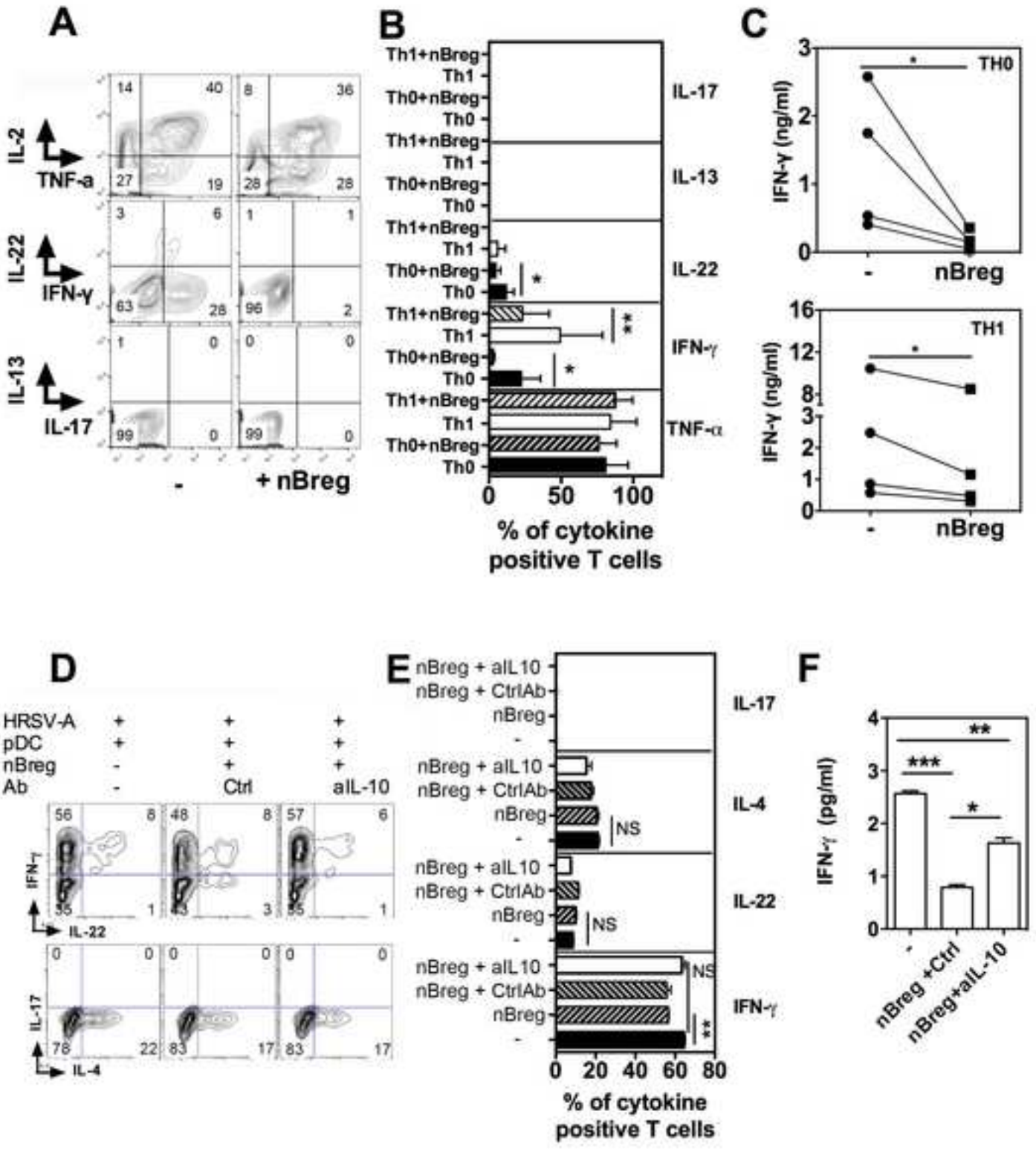

Figure 3

Click here to download Figure Fig3_R4.jpg

Figure 3

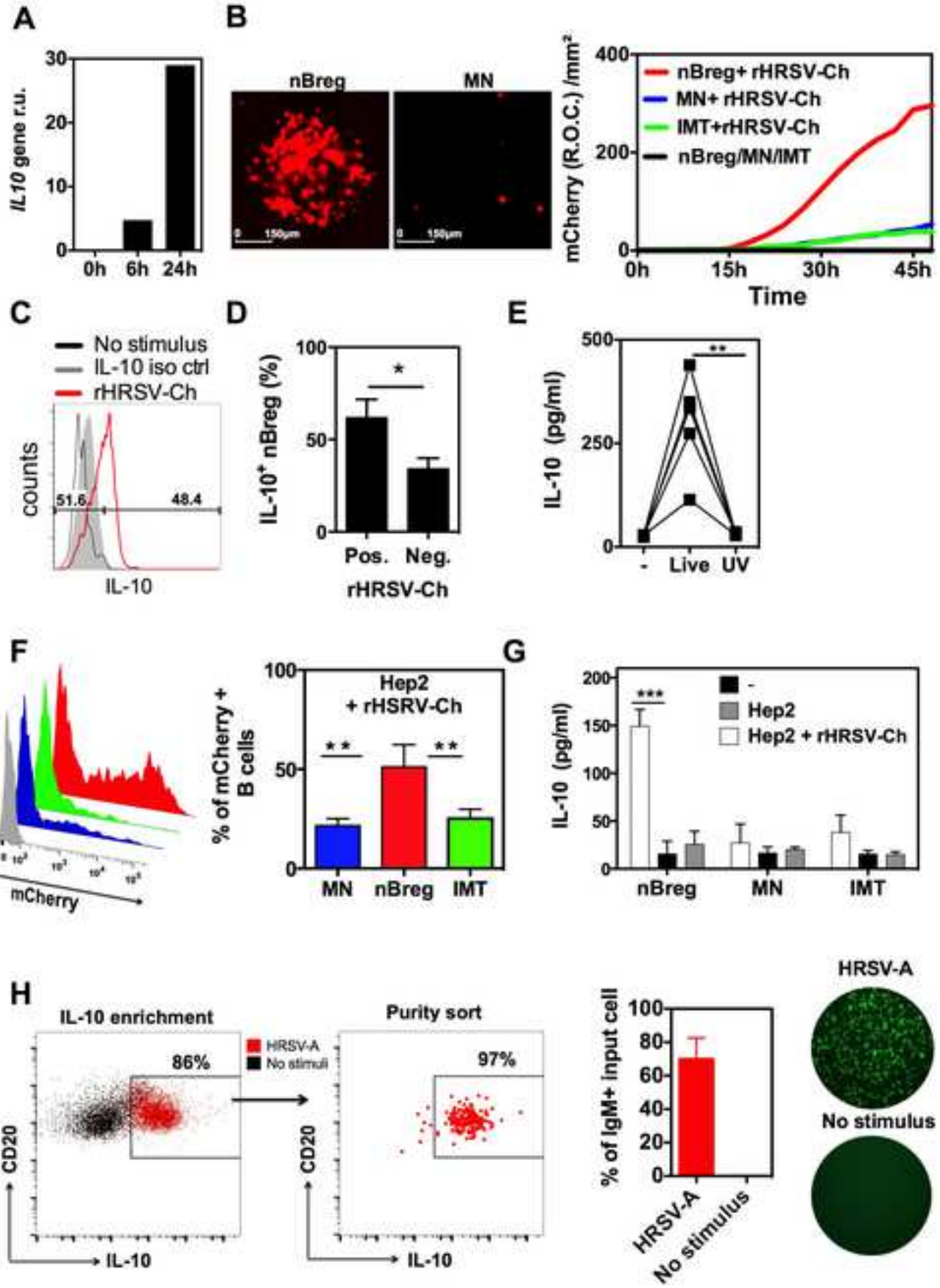

Click here to download Figure Fig4_R4.jpg

Figure 4

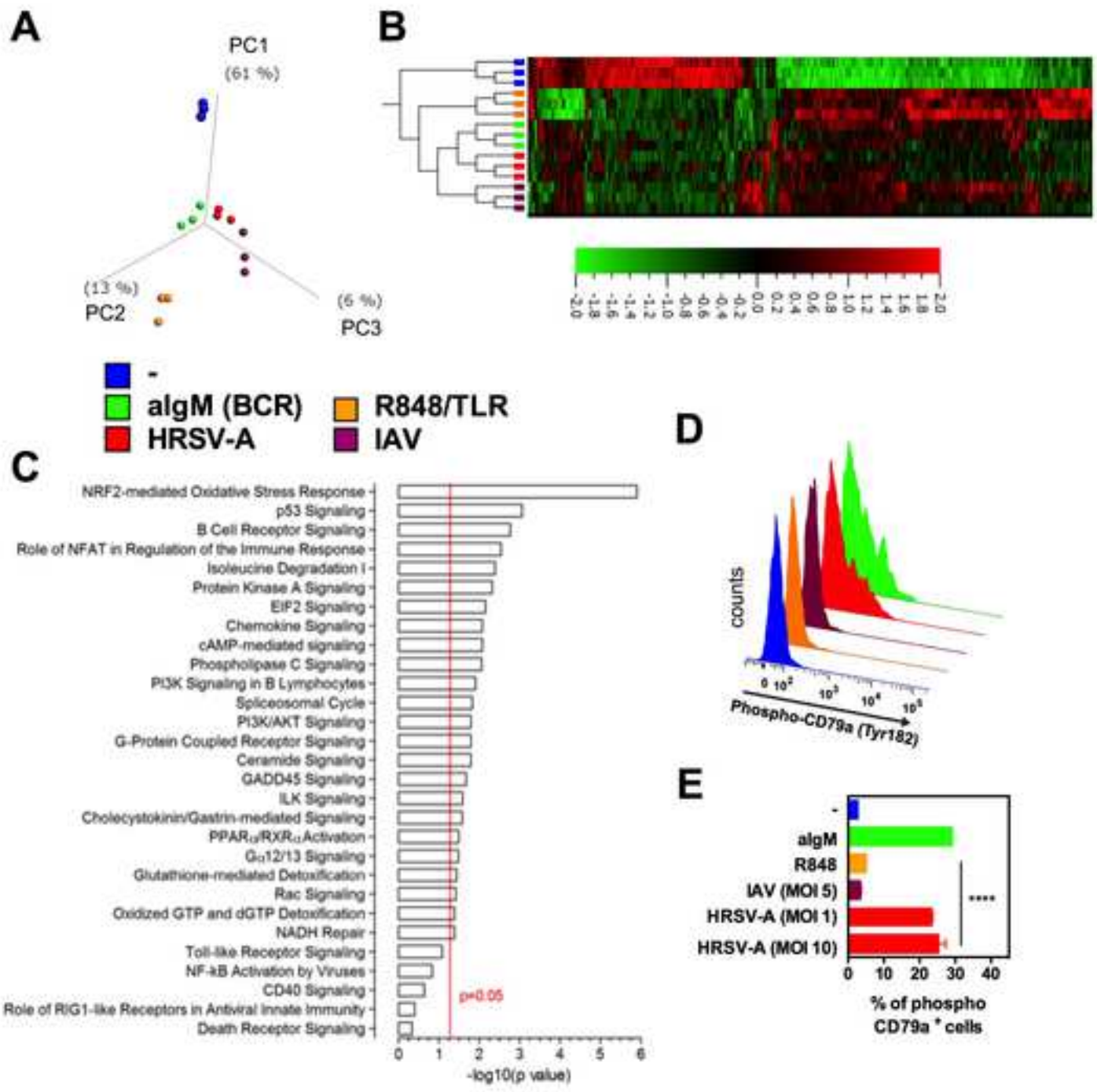

Figure 5

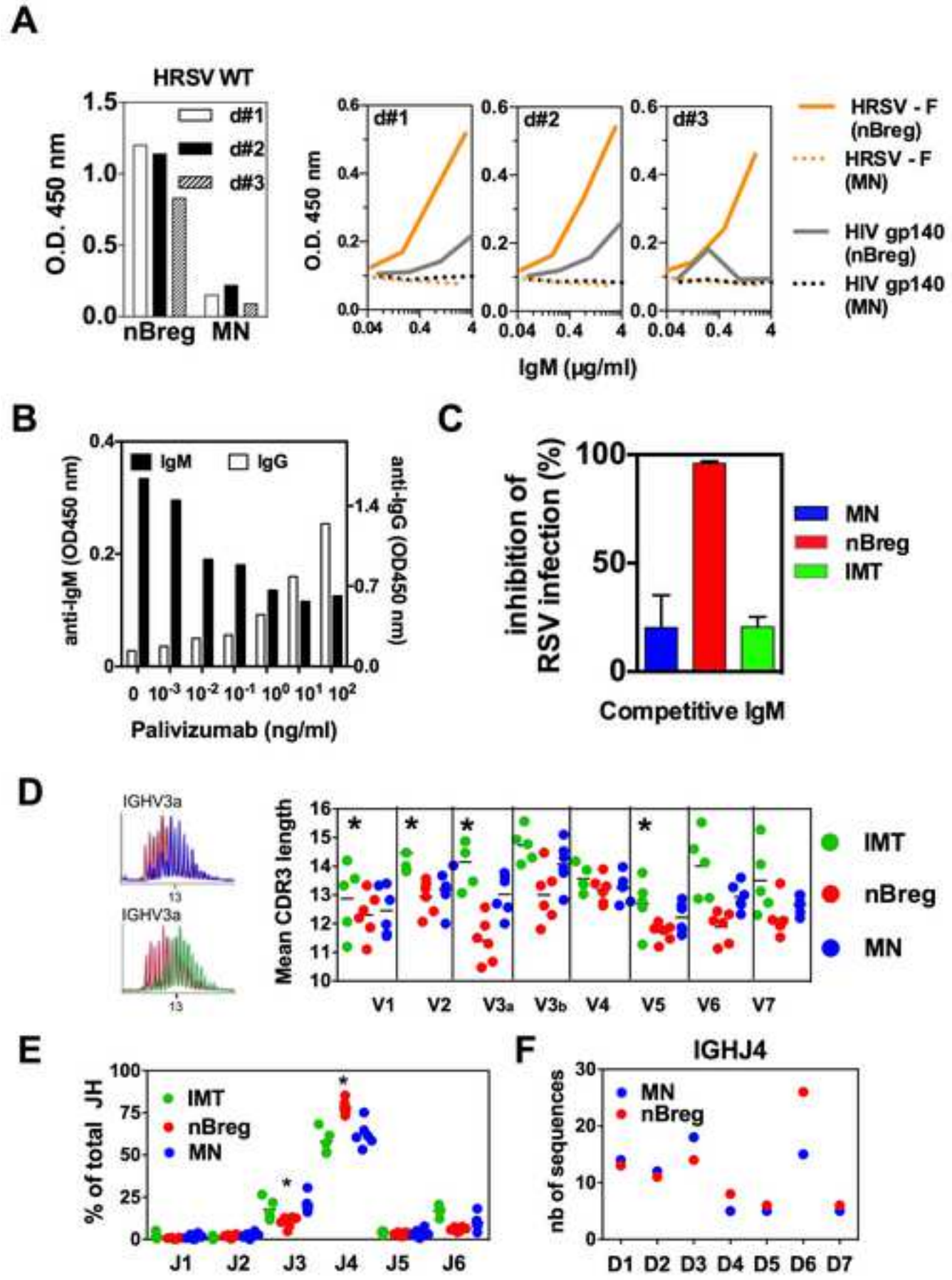

Figure 6

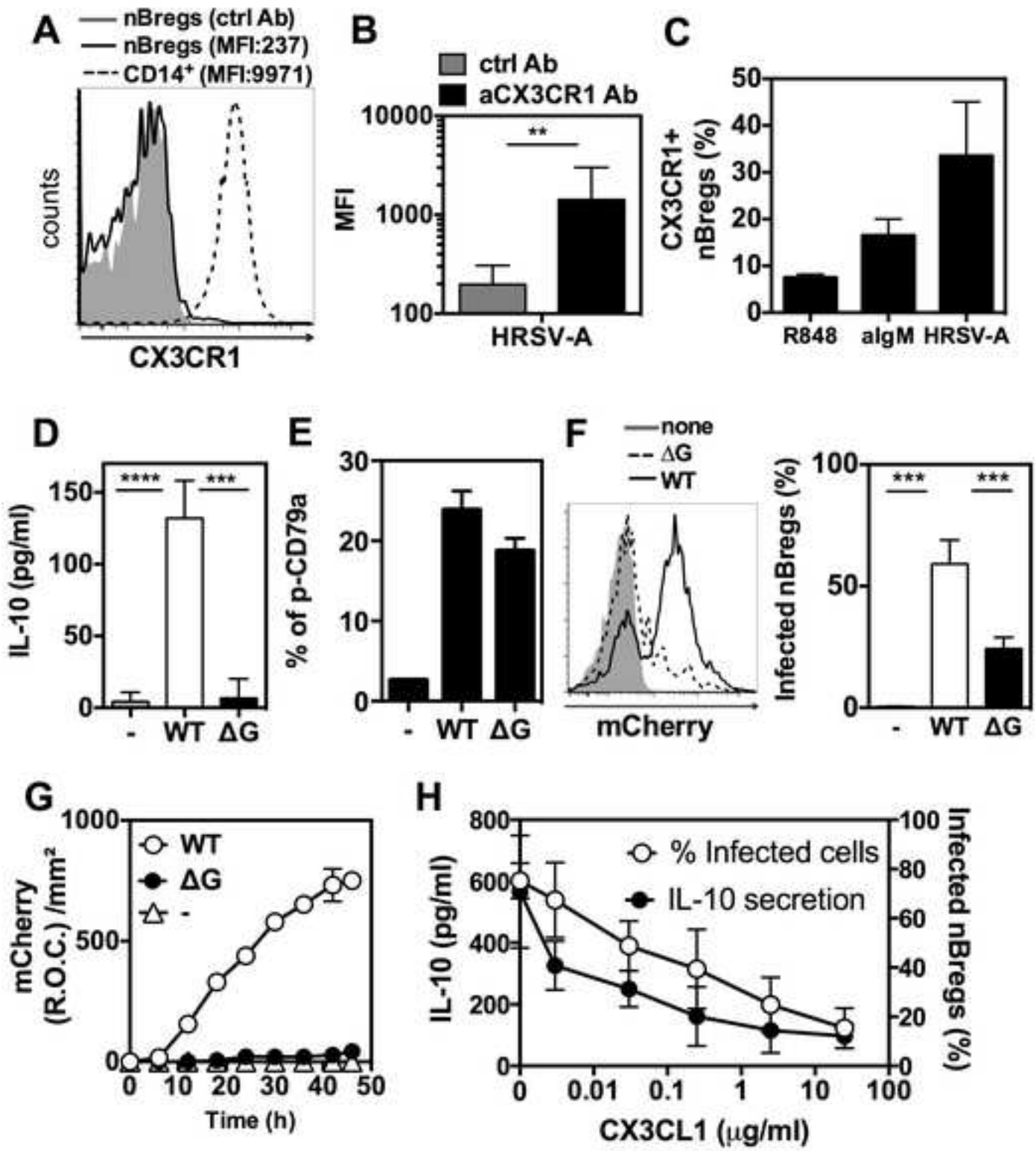

Figure 7

Click here to download Figure Fig7_R4.jpg

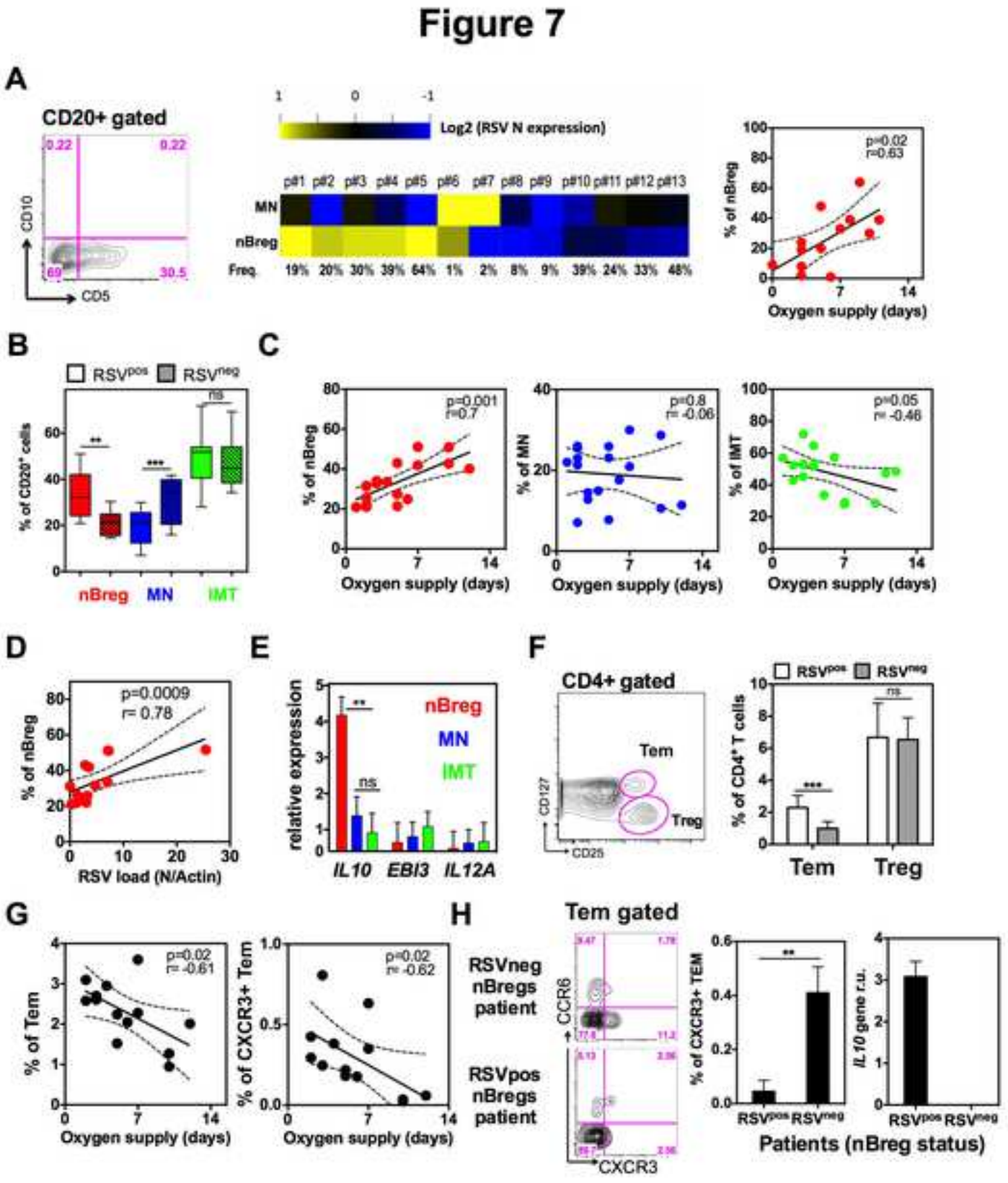

Figure S1

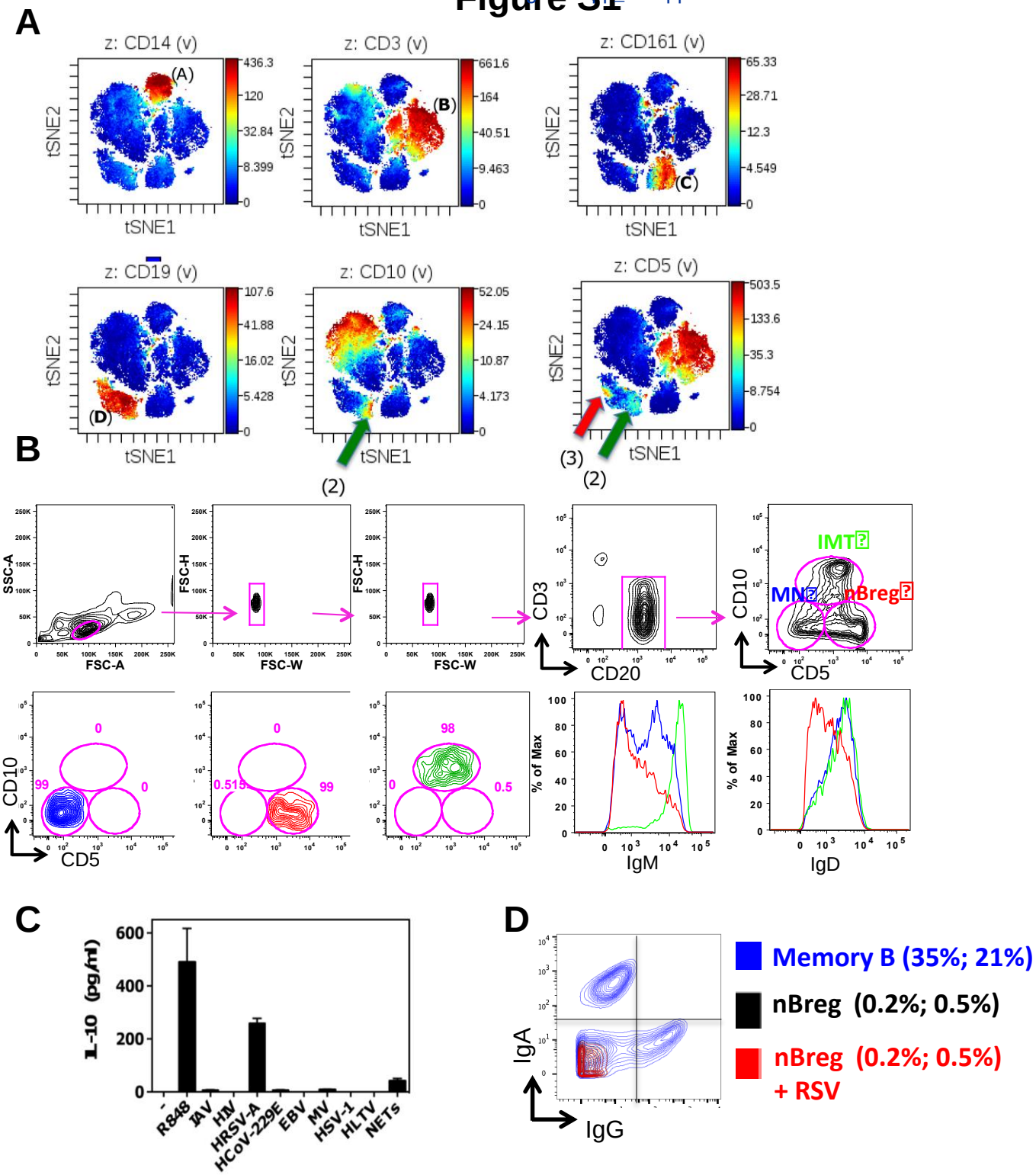

Fig. S1 (related to Fig. 1): viSNE analysis of CBMC

(A) Cord blood cells were analyzed as in Fig. 1A using viSNE which defines based on indicated lineage markers : (A) monocytes, (B) T cells , (C) NK cells, (D) B cells. B cell phenotypes 1, 2 and 3 can be clearly visualized independently of other blood cell types with (2) as $CD10^{pos}CD5^{lo}$ (green arrow) and (3) as $CD5^{hi}CD10^{neg}$ (red arrow). (B) Gating strategy for FACS sorting of neonatal B cells MN , IMT and nBreg, purity check and subsets IgM/IgD expression. (C) 10^5 cord blood nBregs were stimulated with the indicated stimuli. IL-10 was detected in the supernatants at 48 h (means of three donors +/-SD). (D) IgG and IgA detection on nBregs activated or not with RSV in comparison to adult Memory B cells. In parenthesis, frequencies of Ig isotype is indicated (IgA%; IgG%).

Figure S2

A

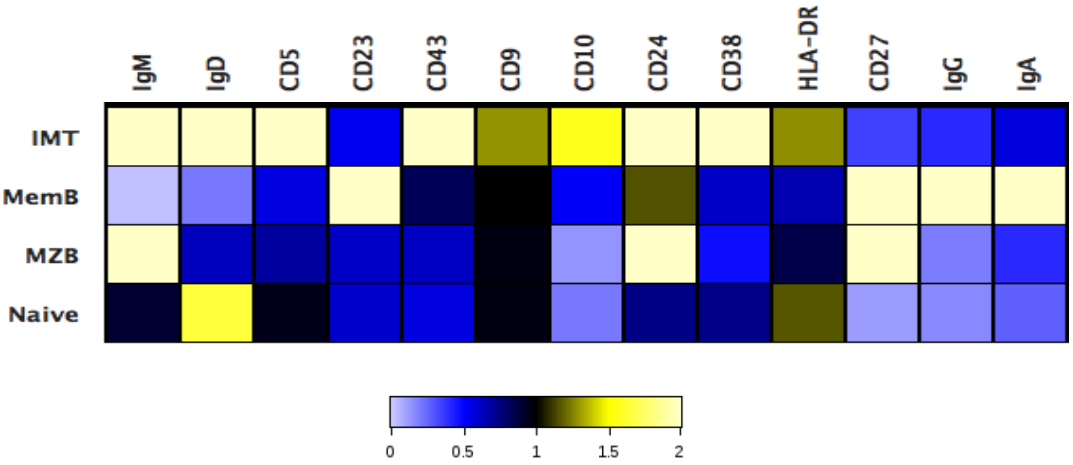

B

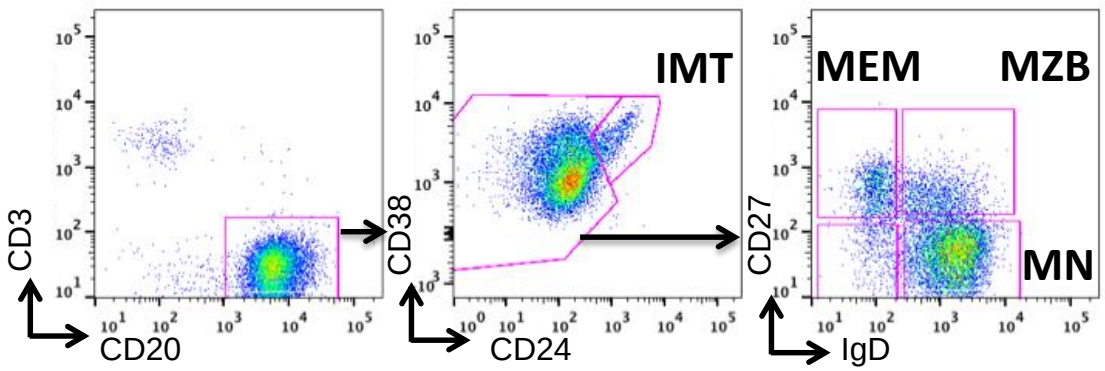

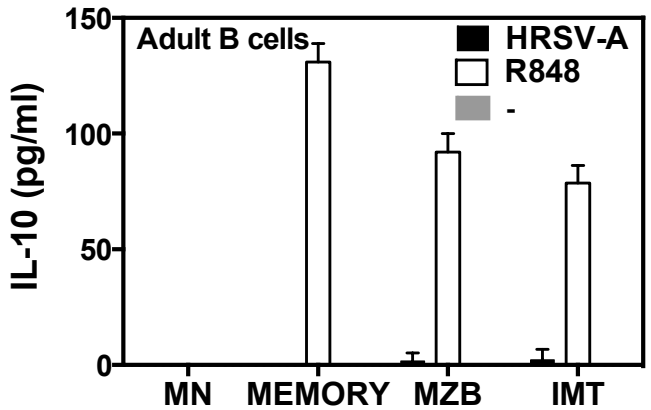

Fig. S2 (related to Fig. 1): IL-10 response of B cells to viruses

(A) CyTOF of adult B cell subsets for the expression of the indicated markers, data were normalized to the the total population of B cells.

(B) 10^5 adult blood B subsets were purified by FACS with indicated gating strategy. Mature Naïve (MN), memory B cells (MEM), marginal zone B cells (MZB) were pre-gated on CD24loCD38+/lo mature B cells, and (IMT) Immature transitional correspond to $CD24^{hi}CD24^{hi}$ B cells. Sorted B cells were then stimulated or not with HRSV-A or R848 and IL-10 was detected at 48h by ELISA. Results are expressed as the means of triplicates+/-SD and are representative of two experiments.

Figure S3

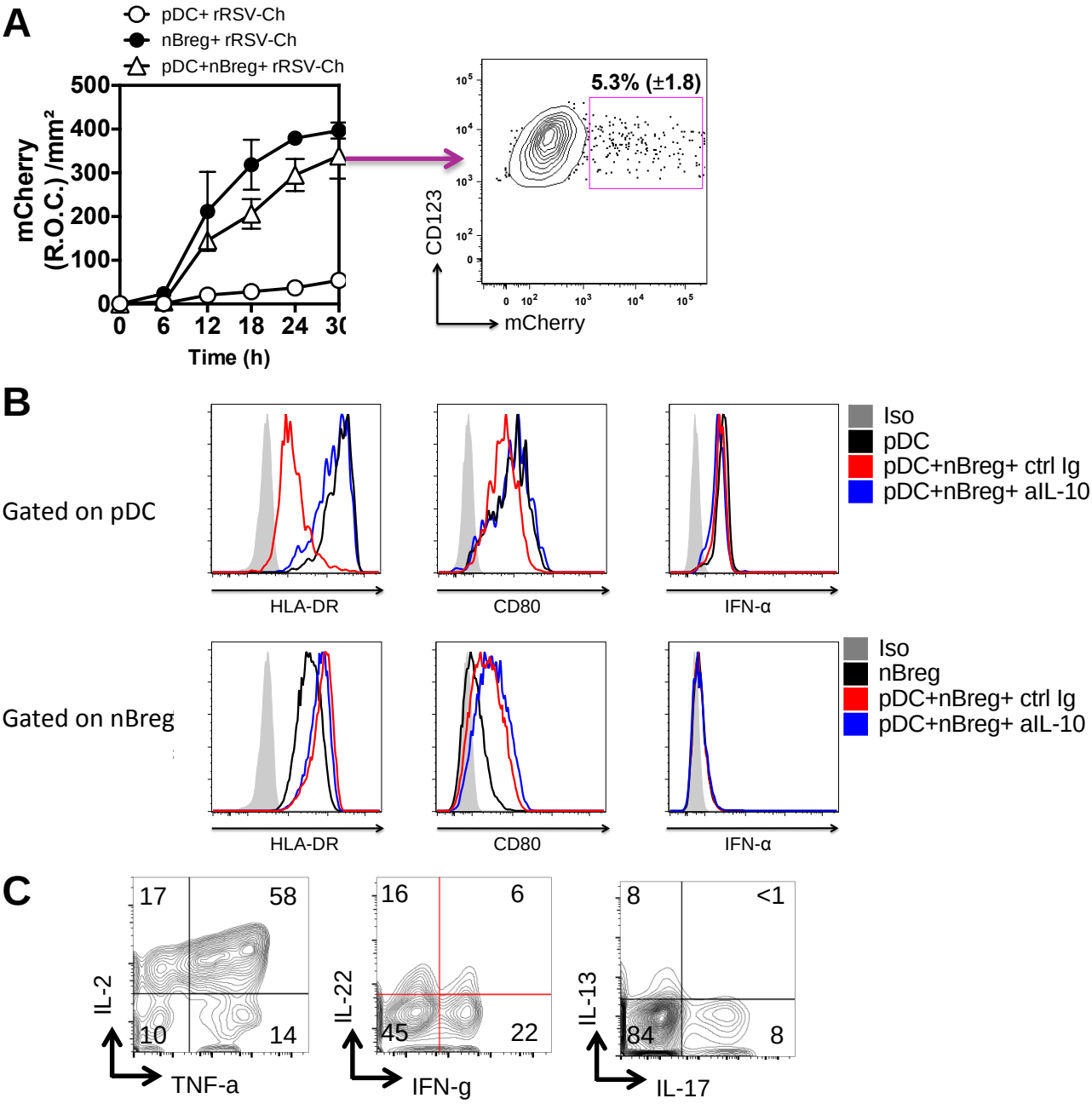

Fig. S3 (related to Fig. 2) :
(A-B) pDC and nBreg cells were sorted from cord blood and cultured with rRSV-Ch (MOI=2.5) alone or in co-culture for 30h-48h in the presence of anti-IL10 (a-IL10) or an isotype control Ig. (A) Left panel represents pDC infection as compared to nBreg cells cultured alone measured by live microscopy. Right panel FACS plot shows the frequency of RSV infected pDC when cultured alone. Results are means of triplicates and are representative of three experiments. (B) Histograms show the expression of HLA-DR, CD80 or intracellular IFN-α after 48h of stimulation with HRSV-A. Iso corresponds to isotype control staining, and ctrl Ig to anti-IL10 isotype control. (C) CD4 naive T cells were culture in TH17 conditions, and serve as positive control of Fig. 2 for intracellular staining of cytokines indicated on the X and Y axes.

Figure S4

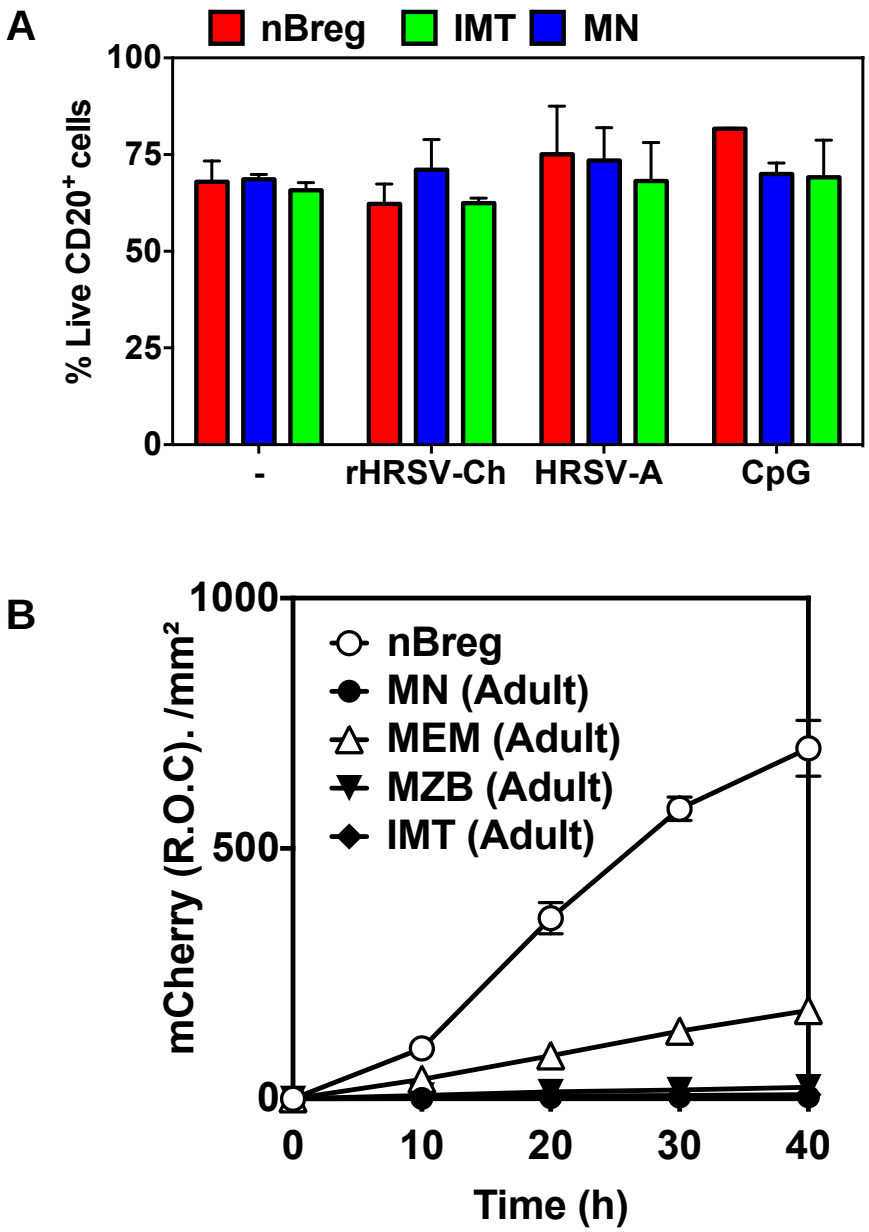

Fig. S4 (relate to Fig. 3)

(A) 10^5 B cell subsets were FACS sorted as nBreg, MN or IMT and stimulated by rHRSV-Ch, HRSV-A or CpG for 48 h. Live/dead cells were analyzed by FACS following DAPI staining. Live cells were negative for DAPI, and results are mean +/-SD of 3 experiments. (B) 10^5 nBregs and adult B cells were sorted as indicated in FigS2B and exposed to rHRSV-Ch (MOI=2.5). Viral infection was assessed mCherry expression using fluorescent live microscopy.

Figure S5

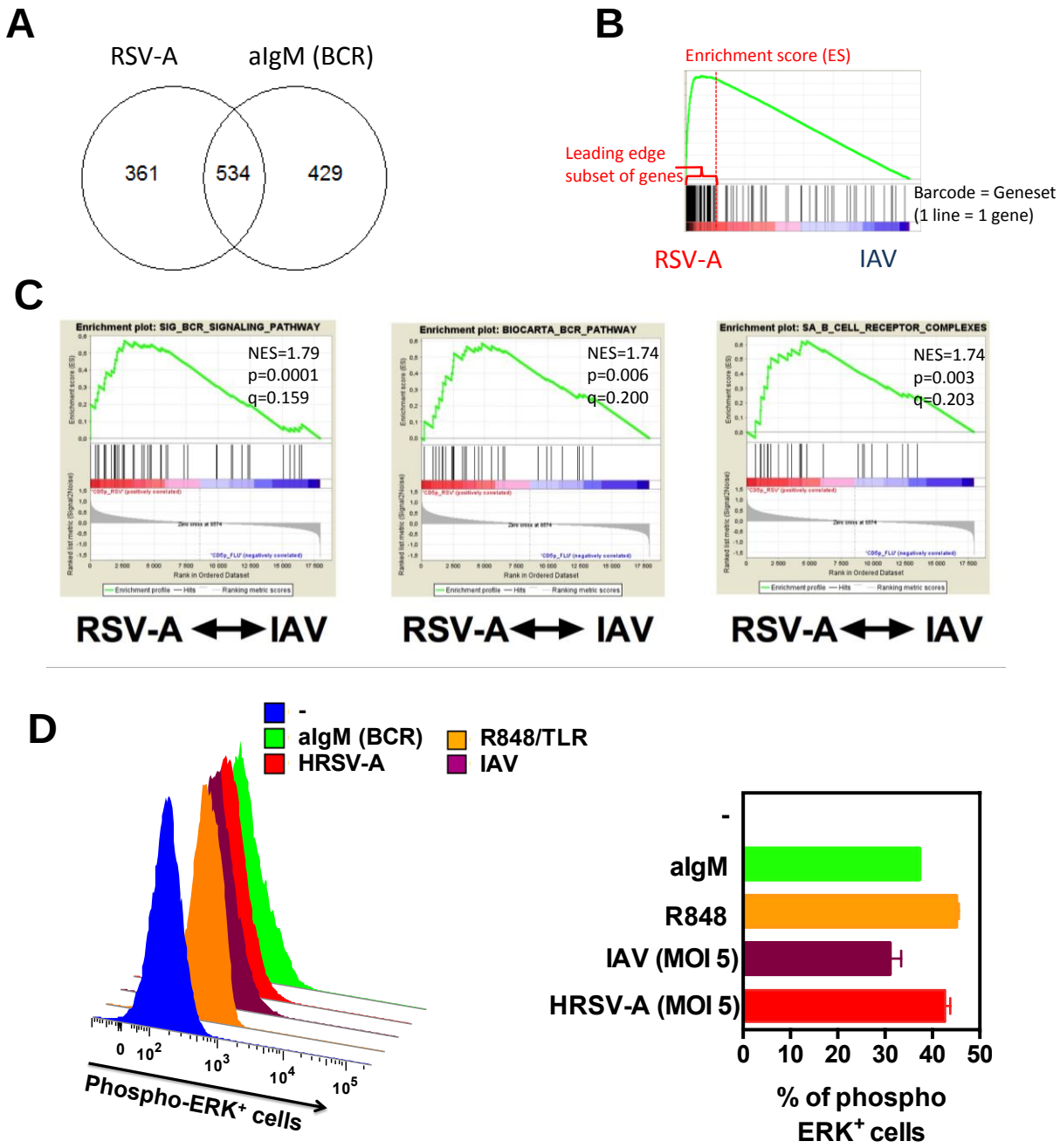

Fig. S5 (related to Fig. 4): Pathway analysis of RSV stimulated nBregs. (A-C) Cord blood nBregs were FACS-sorted as CD19+CD5+CD10- B cells, and they were either left unstimulated (-) or stimulated for 6 h with HRSV-A, IAV or anti-IgM. Gene expression profiles were compared by microarray analysis for 3 independent donors. (A) Venn diagram for the number of common and specific genes activated in nBregs for aIgM (BCR) and RSV. (B-C) GSEA analysis. (B) Description of GSEA analysis plot. (C) GSEA comparison of IAV and RSV activated nBregs for BCR receptor, signaling and molecular pathways. (D) nBregs were activated as indicated for 30 min. and ERK phosphorylation was assessed by FACS. FACS plots and mean of triplicates+/-SD are shown.

Figure S6

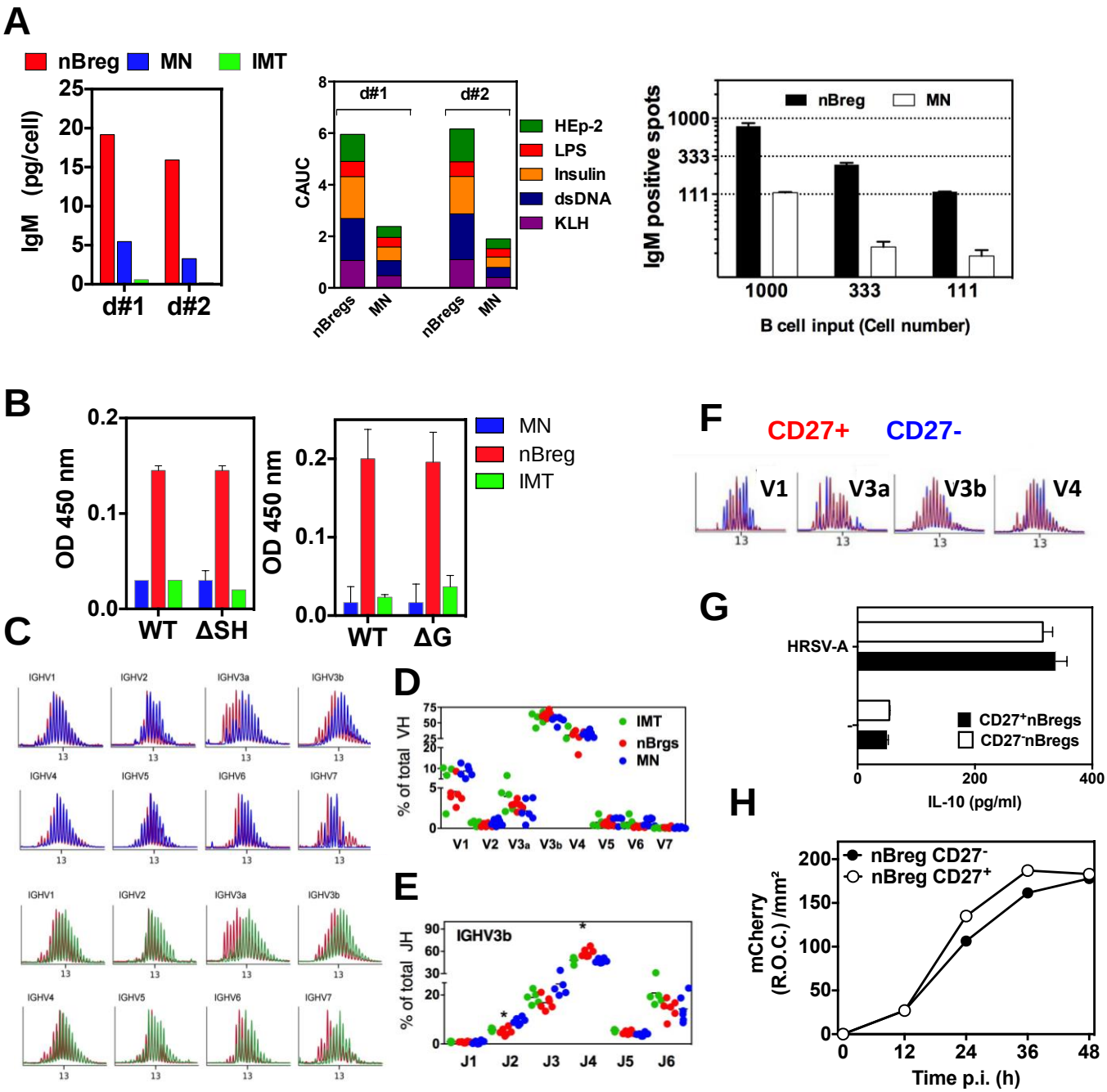

Fig. S6 (related to Fig. 5): B cell reactivity and repertoire analysis

(A) Indicated B cell subset (3X10^6/ml) was stimulated for 6 days with CpG, and concentration of IgM was determined. IgM produced by nBregs and MN were tested at 4-0.4 and 0.04 µg/ml for polyreactivity against the indicated Ag by ELISA and results are plotted as CAUC. Alternatively, B subsets, was analyzed using an enzymatic ELISPOT assay to evaluate the frequency IgM secreting cells after 48 h. (B) IgM (100 ng/ml) produced by nBregs, IMT and MN neonatal B cell were tested by ELISA for recognition of WT HRSV-A vs. (B) ΔSH and (C) ΔG mutants. (C) CDR3 length profiles (in AA) of one neonatal sample nBreg subset (red) for the various IGVH are compared by overlay with MN (blue) and IMT (green) B cell subsets. For the three neonatal B cell subsets, (D) the IgM V usage and (E) the J usage repertoire was analyzed for IgM V3b (IGHV3b) (*P<0.05). Each dot represents one donor (n=5). (F-H) nBregs were sorted as CD27-positive and negative cell fractions and subjected to repertoire analysis as in Fig. 5 and to RSV infection and IL-10 response. CDR3 length spectra are shown for major IGHV gene family (V1, V3a, V3b and V4). (G) nBregs subsets were exposed to HRSV-A and IL-10 was detected by ELISA at 48 h. (H) nBregs subsets were exposed to rHRSV-Ch and infection was monitored by following mCherry expression by fluorescent live microscopy for 48h.

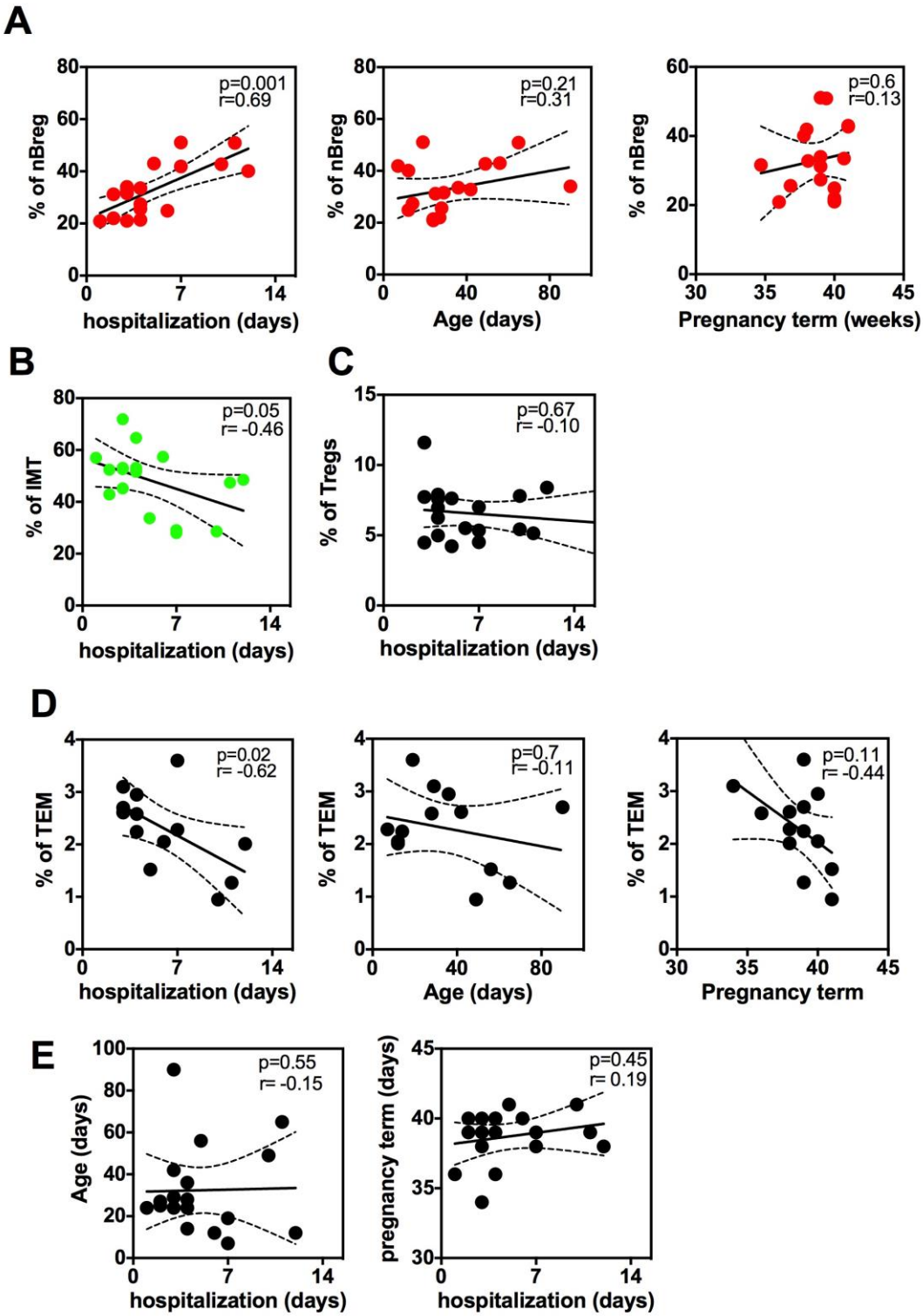

Figure S7 (related to Fig. 7) : RSV-positive patient cohort analysis. Correlation analysis of blood cell parameters of patients suffering of acute bronchiolitis with duration of ICU hospitalization, age of patients and pregnancy term. Immunological parameters correspond to those presented in Figure 7.

Supplementary Experimental procedures

HRSV mutants

To generate the rHRSV-ΔG-Cherry virus, the first ATG of the G gene was substituted by ACA by site-directed mutagenesis using the QuickChange II site-directed mutagenesis kit (Stratagene). Mutagenesis was performed using the pJET2.1 vector in which the HRSV G gene was cloned at XhoI-StuI sites, with the following primers: forward primer: CGTTGGGGCAAATGCAAACACATCCAAAAA CAAGGACCAACGC; reverse primer: GCGTTGGTCCTTGTTTTTGGATGTGTTTGCATTTGCC CCAACG (sequence changes were boxed). The modified sequence was then sub-cloned in the pACNR-rHRSV-Cherry vector (Genbank accession N° KF713492.1) to engineer the pACNR-rHRSV-ΔG–Cherry vector. Sequence analysis was carried out to control the integrity of this vector. The recombinant rHRSV-ΔG-Cherry virus was recovered by co-transfecting the pACNR-rHRSV-ΔG–Cherry vector together with plasmids expressing the RSV N, P, M2-1 and L proteins in BSRT7/5 cells (Buchholz et al., 1999) as previously described (Rameix-Welti, 2014). Rescued viruses were passaged and amplified on Vero cells grown at 37°C with 5% CO_2 in EMEM (Gibco) supplemented with 2% foetal calf serum (FCS). To control that rHRSV-ΔG–Cherry no longer express G, immunofluorescence was carried out after virus titration on Vero cells (described below). Briefly, 6 days postinfection cells were wash with PBS 1X, fixed with PBS- PFA 4% and labelled with either a polyclonal anti-N serum (Castagne et al., 2004) or anti-G monoclonal antibodies (AbD Serotec). Fluorescent plaques were observed using an inverted fluorescence microscope. For rHRSV-ΔSH, SH gene together with corresponding Gene Start and Gene End signals was deleted from the full-length cDNA clone of HRSV subgroup A previously described (Rameix-Welti et al., 2014) using standard cloning procedures. Resulting sequence is available in the Genbank nucleotide database with accession code KU707921. rHRSV-ΔSH was rescued and amplified as previously described. Viral genome sequence was verified at passage 3. Viruses were titrated on Vero cells at 37°C using a plaque assay procedure derived from the one previously described (Rameix-Welti et al., 2014).

RSV detection in nasal washes.

For RSV expression, B cell subsets were directly sorted from the nasal washes in a Lysis Solution (Lysis Enhancer and Resuspension Buffer at a ratio 1:10) (CellsDirect™ One-Step qRT-PCR Kit, Invitrogen). Sequence-specific pre-amplification was performed using TaqMan PreAmp Master Mix (Invitrogen). Unincorporated primers were inactivated by Exonuclease I treatment (New England Biolabs). RSV nucleoprotein gene N analysed by qPCR with 2x Sso Fast EvaGreen Supermix With Low ROX (Bio-Rad Laboratories) using primers in 48:48 Dynamic Arrays on a Biomark System (Fluidigm). Quantitative data for the viral N was normalized to house keeping genes mRNA content (β-actin and GAPDH). *RSV N* forward primer AGATCAACTTCTGTCATCCAGCAA and reverse primer TTCTGCACATCATAATTAGGAG TATCAAT were used.

B cell repertoire analysis.

We characterized the IgM repertoire at the molecular level in various B-cell subsets from cord blood. IGHV gene usage and CDR3 analysis were performed using the Immunoscope method coupled with real-time PCR to provide quantitative information on the IGHV and IGHJ gene usage. Briefly, PCR reactions were performed by combining a primer and a specific fluorophore-labeled probe for the constant region CHμ with one of eight primers covering the different IGHV1-7 genes. V3 was divided in two subgroups: V3a (V3-15,49,72,73) and V3b (V3-d,07,09,11,13,20,21,23,30,30.3,33,43, 48,53,64,66,74). Reactions were performed using Taqman 7300. PCR products were subjected to run-off reactions with a nested fluorescent primer specific for the constant region gene. The fluorescent products were separated and analyzed on an ABI-PRISM 3730 DNA analyzer to determine CDR3 lengths. The IGHV3a/C amplification products were cloned, sequenced, and analyzed according to the procedure described previously (Lim et al., 2008). A more detailed analysis of V-Cμ H-chain transcripts was performed to examine the usage of IGHD families and the IGHJ gene as well as the

of the IGHV-D and IGHJ-IGHD junction regions. IMGT/junction analysis was used to accurately identify the different regions of the junctions: 3'V-region, D-region(s), and 5'J-region. IGVH CDR3 length was analyzed in nBregs, and NM B cells. Each profile represents the CDR3 length distribution for a given IGVH family. One-way ANOVA was used for group comparisons; P values <0.05 were considered statistically significant. List of primers is detailed below.

Polyreactivity ELISA

IgM (3-4ug/ml) from nBregs or MN were tested for polyreactivity using high-binding 96-well ELISA plates (Costar) coated with 10 μg/ml of LPS from E. coli (Sigma, L2637), Keyhole Limpet Hemocyanin (KLH) (Sigma, H8283), ssDNA from dsDNA (heated at 95°C for 30 min), 5 μg/ml Human insulin (Sigma, I9278), HEp-2 whole cell lysates (Prigent et al., 2016) and purified HIV-1 (YU-2) gp140 trimers gp140 (Mouquet et al, 2011). (2.5μg/ml). ELISA done as previously described. HRSV-F protein (4μg/ml) was described (McLellan et al., 2011 ; McLellan et al., 2013)

Buchholz, et al. J Virol *73*, 251-259.
Castagne, N.,et al. The Journal of general virology *85*, 1643-1653.
Lim, A. et al. Int Immunol *20*, 105-116.
McLellan, et al. Science 340 (6136): 1113–17. doi:10.1126/science.1234914.
McLellan et al. Journal of Virology 85 (15): 7788–96. doi:10.1128/JVI.00555-11.
Rameix-Welti, M.A. et al. Nature communications *5*, 5104.
Prigent, J. et al., European journal of immunology *46*, 2340-2351.
Mouquet, H. et al. PloS one *6*, e24078.

Supplentary Experimental procedures are related to reagents and info of the experimental procedure

List of V, J and Cmu specific primers for repertoire analysis.

	Primer Sequence	Specificity	Location
IGHV subgroup			
V1	AGTGAAGGTCTCCTGCAAGGC	V1-02,08,18,58,69,e	FR1
	AGTGAAGGTTTCCTGCAAGGC	V1-03,45,46	FR1
	AGTGAARRTCTCCTGCAAGGT	V1-f,24	FR1
V2	AACCCACASAGACCCTCAC	V2-05,70,26	FR1
V3a	GCAGATTCACCATCTCAAGAGATG	V3-15,49,72	FR3
	GCAGGTTCACCATCTCCAGAGATG	V3-73	FR3
V3b	GCCGATTCACCATCTCCAGAGA	V3-07,09,13,20,21,30,30.3 33,43,48,53,74	FR3
	GCAGATTCACCATCTCCAGAGA	V3-d,64,66	FR3
	GCCGATTCACCATCTCCAGGGA	V3-11	FR3
	GCAGGTTCACCATCTCCAGAGA	V3-23	FR3
V4	CTACAACCCGTCCCTCAAGAGT	V4-04,28,30-2,30-4,31,34,b	FR3
	CTACAACCCCTCCCTCAAGAGT	V4-59,61	FR3
V5	GTGAAAAAGCCCGGGGAG	V5-51,a	FR1
V6	TCCGGGGACAGTGTCTCT	V6-01	FR1
V7	GGTGCAATCTGGGTCTGAGT*T*	V7-04.1	FR1
IGHJ subgroup			
J1	CCCTGGCCCCAGTGCT*G	J1	
J2	CCACGGCCCCAGAGATC*G	J2	
J3	CCCTTGGCCCCAGAYATCAAAA*G	J3a,b	
J4	GGTTCCTTGGCCCCAGTA*G	J4a	
	GGTTCCCTGGCCCCAGTA*G	J4b	
	GGTCCCTTGGCCCCAGTA*G	J4d	
J5	TGGCCCCAGGRGTCGAA*C	J5a,b	
J6	CCTTGCCCCCAGACGTCCA*T	J6a	
	CCTTGGCCCCAGACGTCCA*T	J6b	
	CCTTTGCCCCAGACGTCCA*T	J6c	
IGH mu chain			
	CAGCCAACGGCCACGC	IGHM.01,02,03	CH1
	6Fam-GGAGACGAGGGGGAAAAGG		CH1
	6Fam-CCGTCGGATACGAGC-MGB		CH1

Supplentary Experimental procedures are related to reagents and info of the experimental procedure

Demographic and diagnostics data of children

	RSV group	positive	negative
Diaganostics	RSV+	36	10
	Other viruses	0	0
	Bacteria	6	0
Sampling	Blood	29	10
	NPA	13	0
Age (months)	median	1.18	1.15
	IQR	0.63-1.73	0.16-2.03
Gestational age at birth (weeks)	median	39	38
	IQR	38-40	37-39.29
Weight (kg)	median	4.0	3.9
	IQR	3.34-5.03	3.46-4.65

Supplentary Experimental procedures are related to reagents and info of the experimental procedure

List of antibodies used for mass cytometry

141 Pr	CD196	REA190	Miltenyi
142 Nd	CD19	LT19	Miltenyi
143 Nd	CD11c	mj4-27g12	Miltenyi
143 Nd	CD123	AC145	Miltenyi
143 Nd	CD56	REA196	Miltenyi
143 Nd	IgA	IS11-8E10	Miltenyi
144 Nd	CD38	IB6	Miltenyi
145 Nd	CD4	RPT-T4	Biolegend
146 Nd	CD161	191B8	Miltenyi
146 Nd	CD20	LT20	Miltenyi
146 Nd	CD8	BW135/80	Miltenyi
147 Sm	CD11b	M1/70.15.11.5	Miltenyi
147 Sm	CD20	LT20	Miltenyi
148 Nd	CD86	FM95	Miltenyi
149 Sm	CD15	VIMC6	Miltenyi
150 Nd	CD10	97C5	Miltenyi
150 Nd	CD304	AD5-17F6	Miltenyi
151 Eu	CD70	REA292	Miltenyi
151 Eu	CD5	AC145	Miltenyi
152 Eu	CD23	M-L23,4	Miltenyi
152 Eu	CD4	VIT4	Miltenyi
153 Eu	CD62L	145/15	Miltenyi
154 Sm	CD27	M-T271	Miltenyi
158 Gd	CD40	HB14	Miltenyi
159 Tb	CD197	REA108	Miltenyi
159 Tb	CD9	SN4	Miltenyi
160 Gd	CD14	TUK4	Miltenyi
161 Dy	CD33	AC104.3E3	Miltenyi
162 Dy	CD11c	mj4-27g12	Miltenyi
164 Dy	CD15	VIMC6	Miltenyi
164 Dy	CD161	191B8	Miltenyi
164 Dy	CD56	REA196	Miltenyi
165 Ho	CD43	DF-T1	Miltenyi
166 Er	CD24	32D12	Miltenyi
167 Er	CD5	UCHT2	Miltenyi
168 Er	CD138	44F9	Miltenyi
169 Tm	CD45RA	T6D11	Miltenyi
169 Tm	IgG	IS11-3B2.2.3	Miltenyi
170 Er	CD3	UCHT1	Biolegend
172 Yb	anti-IgM	PJ2-22H3	Miltenyi
173 Yb	CD21	HB5	Miltenyi
173 Yb	CD40	HB14	Miltenyi
174 Yb	anti-IgD	IgD26	Miltenyi
174 Yb	HLA-DR	AC122	Miltenyi
175 Lu	CD10	97C5	Miltenyi
175 Lu	HLA-DR	AC122	Miltenyi
176 Yb	CD1c	AD5-8E7	Miltenyi

Supplentary Experimental procedures are related to reagents and info of the experimental procedure

Erk1/2 (T202/Y204)	MILAN8R	eBioscience
CXCR3	G025H7	Biolegend
CX3CR1	2A9-1	Miltenyi Biotec
CCR6	11A9	BD
CD10	ebioCB-CALLA	eBioscience
CD123	6H6	eBioscience
CD127	ebioRDR5	eBioscience
CD14	HCD14	Biolegend
CD19	J3-129	eBioscience
CD20	2H7	eBioscience
CD25	BC96	Biolegend
CD27	L128	BD
CD3	OKT3	eBioscience
CD304	AD5-17F6	Miltenyi Biotec
CD4	RPA-T4	eBioscience
CD45RA	HI100	Biolegend
CD45RO	UCHL1	eBioscience
CD5	L17F12	eBioscience
CD79a (Tyr182)	D1B9	Cell signaling technology
IFN-g	45.B3	Biolegend
IL-4	MP4-25D2	BD
IL-13	JES10-5A2	Biolegend
IL-17A	BL168	Biolegend
IL-22	22URTI	eBioscience
TNF-a	MAb11	eBioscience
IL-10	JES3-9D7	eBioscience
IFN-a	LT27:295	Miltenyi Biotec
CD80	2D10	Biolegend
HLA-DR	L243	Biolegend